FREQUENCY STABILIZATION OF AN OPTICAL FDM SYSTEM

by

Diane Shan-Yuan Ho

S.B. Massachusetts Institute of Technology

(1986)

SUBMITTED IN PARTIAL FULFILLMENT

OF THE REQUIREMENTS FOR THE

DEGREE OF

MASTER OF SCIENCE

IN ELECTRICAL ENGINEERING AND COMPUTER SCIENCE

at the

MASSACHUSETTS INSTITUTE OF TECHNOLOGY

May 1990

Signature of Author _____

Department of Electrical Engineering and Computer Science
May 29, 1990

Certified by _____

Pierre A. Humblet
Thesis Supervisor

Accepted by _____

Arthur C. Smith
Chairman, Departmental Commitee on Graduate Students

FREQUENCY STABILIZATION OF AN OPTICAL FDM SYSTEM

by

Diane Shan-Yuan Ho

SUBMITTED IN PARTIAL FULFILLMENT
OF THE REQUIREMENTS FOR THE
DEGREE OF
MASTER OF SCIENCE
IN ELECTRICAL ENGINEERING AND COMPUTER SCIENCE
MAY 1990

Abstract

Optical frequency division multiplexing communication systems have the potential for a large throughput. However, semiconductors lasers used as optical sources have random frequency fluctuations that deteriorate system performance. Hence, frequency monitoring and stabilization are necessary to prevent channel interference.

A mathematical model was formulated to evaluate the performance of a frequency stabilization feedback scheme to lock many optical frequency shift keyed signals onto distinct resonances of a single Fabry-Perot resonator. The optimal and suboptimal loop filters to minimize the mean squared error were found, and performance was evaluated as a function of the system parameters.

Thesis Supervisor: Pierre A. Humblet
Title: Associate Professor of Electrical Engineering

Acknowledgements

"When you drink from the stream remember the spring."
-Chinese Proverb

My deepest gratitude to Professor Humblet for his guidance, generosity, and patience. I have truly learnt much about how to do research from him through his insightfulness, brilliance, and kindness. Sincere appreciation to Professor Gallager for his words of wisdom and advice.

Heartfelt thanks to my officemates and friends: Ying Li, Emre Telatar, Nancy Lee, Rajesh Pankaj, John Spinelli, Whay Lee, Jane Simmons, Rick Barry, David Tse, Tom Richardson, Murat Azizoğlu, Daniel Lee, Roy Yates, Diana Dabby, Abhay Parekh, Walid Hamdy, and Evan Wang for all their help, support, encouragement, and jokes. You guys are the greatest.

Special thanks to Emre and Ying for their expert computer help with this thesis.

To my family, you are my blood and my soul... nothing can justly express my gratitude .... To Shan-Ping and Tom, your examples have always been an encouragement. To Della and Peter, you are are indeed a joy to my heart. To Mother and Father, you are truly "the wind beneath my wings."

The hand of the Lord was upon me, and he brought me out by the Spirit of the Lord and set me in the middle of the valley; it was full of bones. he led me back and forth among them, and I saw a great many bones on the floor of the valley, bones that were very dry. He asked me, "Son of man, can these bones live?"

I said, "O Sovereign Lord, you alone know."

Then he said to me, "Prophesy to these bones and say to them, 'Dry bones, hear the word of the Lord! This is what the Sovereign Lord says to these bones: I will make breath enter you, and you will come to life. I will attach tendons to you and make flesh come upon you and cover you with skin; I will put breath in you, and you will come ot life. Then you will know that I am the Lord."

So I prophesied as I was commanded. And as I was prophesying, there was a noise, a rattling sound, and the bones came together, bone to bone. I looked, and tendons and flesh appeared on them and skin covered them, but there was no breath in them.

Then he said to me, "Prophesy to the breath; prophesy, son of man, and say to it, 'This is what the Sovereign Lord says: Come from the four winds, O breath, and breathe into these slain, that they may live.' " So I prophesied as he commanded me, and breath entered them; they came to life and stood up on their feet—a vast army.

I will put my Spirit in you and you will live.

Ezekiel 37:1–10,14

Contents

List of Figures

Chapter 1

Introduction

1.1 Background

Communication systems are moving toward single mode optical fiber for transmission, because they are excellent for point to point communication. The advantages that optical transmission (optical fibers) have over electrical transmission (electrical cables) are the high available bandwidth, low attenuation, low weight, noise immunity, and elimination of ground loops. The move is toward local communication systems connected by various types of networks. Presently, signals are generated and manipulated electrically. Hence, there is an electrical-to-optical conversion at the input (transmitter) to the fiber and optical-to-electrical conversion at the output of the fiber(receiver). Two common light sources are Light Emmitting Diode (LED) which transmits incoherent light and is intensity modulated, and the more expensive Semiconductor Injection Laser which transmits almost coherent light and can use various types of modulation. The laser is modulated by varying the injection current (performed by electronics), changing the temperature, or by varying the cavity mechanically, or using external modulation. The semiconductor laser has frequency fluctuations due to variations in temperature, variations in injection current, and quantum effects. These fluctuations becomes a significant issue for both coherent and incoherent communication systems.

Because tunable heterodyne can demultiplex optical carriers with fine resolution,

Frequency Division Multiplexing (FDM) seems promising in making use of the wide bandwidth of single-mode fiber (approximately 30 THz), since it provides narrow channel spacing. Laser frequency stability is crucial to prevent channel interference. In heterodyne-type optical communication systems, a difficulty is the frequency drift of the lasers, because the semiconductor laser is used as the local oscillator besides the transmitter.

1.2 Optical Communication System

The classical network topologies of bus, loop, and star are also popular fiber optic networks, but they are implemented differently. A star-type network example is shown in Figure (1.1). All tranceivers can communicate with each other. Compared to bus or loop, the star network can have more tranceivers because of lower losses (although it requires more wiring). The power (in dB) decays with the logarithm of number of transceivers whereas for the bus it decays linearly. Optical FDM systems using star networks have the potential for large throughput.

Coherent optical communication systems have better performance than conventional intensity modulation/direct detection systems for the following reasons: (1) Coherent detection have improved receiver sensitivity by 10 to 20 dB with respect to direct detection; (2) The greater frequency selectivity is similar to what is possible in Radio frequencies; (3) Tunable optical receivers; (4) There is the choice of different modulation types such as FSK, PSK, DPSK. The most serious problem with coherent communication is the phase noise of the laser which broadens the linewidth and hence, deteriorates the performance of coherent receivers.

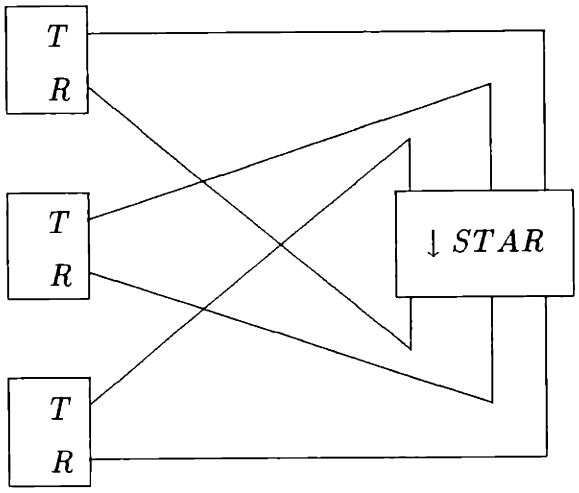

Figure 1.1: Star-Type Optical Network

1.3 Laser Description

A single-mode laser transmitting at frequency f_0 will emit the lasing field

$$E(t) = E_0 e^{-j(2\pi f_0 t + \phi(t))} \tag{1.1}$$

The phase noise $\phi(t)$ is a randon process due to quantum effects and affects the intensity of the laser. These randomly occuring spontaneous emissions which cause phase and intensity changes in the laser field give rise to fluctuations and is called spectral broadening. We would like to know the spectrum of the laser, in particular, the power spectral density of the field, $S_p(f)$, which is the Fourier Transform of the autocorrelation function of $E(t)$, and the power spectral density of the frequency noise $S_F(f)$ (instantaneous frequency fluctuation) $\frac{d}{dt}\phi(t)$.

Henry [1] developed a model to explain the laser noise phenomenon. He assumes that the spontaneous emissions that change the instantaneous phase of the EM field is due to two contributions: (1) Random phase of spontaneous emitted electrons, and (2) consequent change of field intensity which modifies the refractive index of the

medium. The phase is modelled as a random walk process where the steps correspond to the spontaneous emission events that cause a small amount of instantaneous phase change in a random way. Based on this model, he derived the linewidth formula for the power spectral density of the Field spectrum which turns out to be a Lorentzian lineshape shown in Figure 1.2.

The Lorentzian lineshape is proportional to $[\Delta f + (f - f_0)^2]^{-1}$ where f_0 is called the center frequency and is changed by varying the injection current. The Lorentian is the characteristic reponse of damped resonant systems. The linewidth Δf is defined as the separation between the two frequencies where the Lorentzian is at half its maximum peak value. Unfortunately, this Field spectrum widens when the lasing field is modulated.

Experimental measurements show that the frequency noise spectrum has a $1/f$ component in frequency regions below 100 KHz and a Gaussian white noise component that extends to the GHz range, as shown in Figure 1.2. The spectral height, call it A, of the white noise component is related to the linewidth by $A = \Delta f/\pi$. The $1/f$ noise is not Wide Sense Stationary (WSS) because it has no corresponding autocorrelation function. It is part of the relatively low frequency components so can be easily tracked. Hence, our main focus will be on the white component. Furthermore, the effects of this $1/f$ component is not significant for data transmission rates in range 100 Mbits/s to 1 Gbits/s. [6]. Hence, the frequency noise spectrum can be approximated as white for almost all system applications. We will refer to its spectral height as A.

The laser linewidth can be experimentally measured by self-heterodyning. The signal is mixed with a delayed version of itself to produce a spectral image at low frequency. Linewidth measurements can also be obtained by beating the test laser with a much more stable laser, passing the difference signal through a discriminator, and doing a spectral analysis on the output. This can be done by a spectrometer and scanning Fabry-Perot. Experimental measurements show the Lorentian spectrum

of the field (although there is a small resonance peak at the relaxation resonant frequency of the carrier density above 1 GHz), and $1/f$ and white noise components of the frequency spectrum.

Hence, the model of the phase fluctuations used to derive the spectrum of the laser is valid since many experimental measurements agree with the theory.

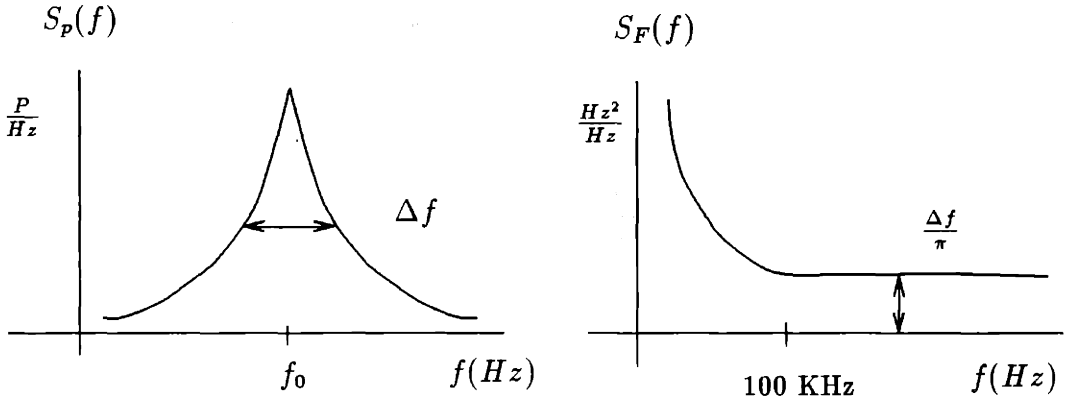

Figure 1.2: (a) Power Spectrum (b) Frequency Spectrum

1.4 Brief Overview of Frequency Stabilization Techniques

Linewidth can be reduced by increasing the quality of the laser. In coherent communication systems, the adverse effects of the linewidth can also be reduced by increasing the data rate since the linewidth requirements are dependent on the rate. Linewidth can be significantly reduced by external feedback (as much as 200 by optical feedback).

Several schemes to stabilize the laser frequency have been developed. All of them use some sort of feedback loop to lock the laser onto a reference frequency via an optical frequency discriminator. This feedback loop controls the laser frequency by varying the injection current (or sometimes temperature). The temperature of the

laser is usually controlled by putting the laser in a Peltier element. The typical stabilization method is shown in Figure 1.3. The frequency discriminator discriminates the frequency deviation of the laser by producing a proportional intensity. Then the photodetector translates this intensity in the optical domain to current. The gain element amplifies the current in proportion to the amount needed to vary that frequency back to center frequency in the laser.

Typical frequency references are Fabry-Perot Interferometers (FPI), fiber-optic ring resonators (FORR), atomic or molecular absorption spectrum, or another reference laser. Frequency discriminators are slopes of the resonance curves or peaks of the FPI of FORR. If the laser is locked to a point on the slope of the reference, then the frequency discriminator is the shape of the slope. If the laser is locked to the peak of the reference, the control signal is generated by demodulating a modulated signal. Then the frequency discrimination function is roughly proportional to the first derivative of the reference lineshape function. The FPI linewidth would be approximately the same order of magnitude as the laser linewidth.

Another type of stabilization scheme is AM sideband injection locking technique [6], where the frequency of the slave lasers are locked to the sideband frequencies of the master laser. The phase of the slave tracks the phase fluctuations of the master. Thus, the linewidth of the slave laser is controlled by injection level and linewidth of the master. The frequency separation of the slave lasers are controlled by the modulation frequency of the master laser.

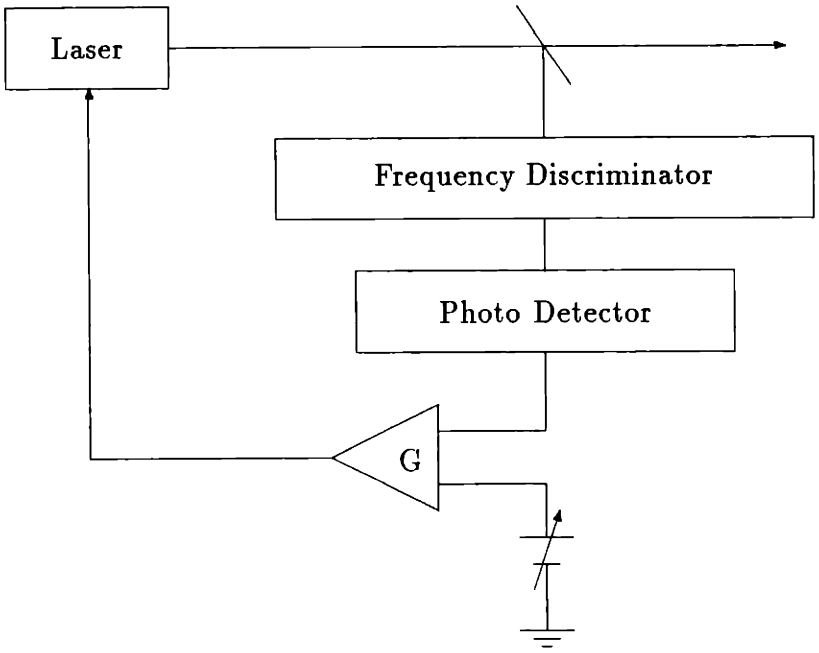

Figure 1.3: Typical Frequency Stabilization Method

Chapter 2

System Model I

2.1 Description of Stabilization Experiment

A novel frequency stabilization scheme for three lasers in an optical, FDM coherent, star network was designed and built by Glance et al. at AT&T Bell Laboratory [4, 5]. Each laser frequency was locked to a distinct resonance of a single fiber Fabry-Perot. If the FDM signals are to be confined to equally spaced frequencies, then lasers must be locked to adjacent resonances or the same number of resonances apart. The stabilization scheme and experiment are described as follows and shown in Figure 2.1.

The three optical sources are fast frequency-tunable external cavity lasers, frequency tuned over 4,000 GHz, transmitting around 1.28μm. Each is frequency-shift-keyed (FSK) at 45 Mbits/s, but can modulate up to 100 MHz. The bit streams are independent random Non-Return-to Zero (NRZ), with modulation index approximately equal to one. The three lasers are combined by a 4×4 fiber star coupler. One of the outputs of the 4×4 coupler will be used in the stabilization feedback loop, consisting of a Fabry-Perot resonator, photodiode, simple electronics, and LPF (low pass filter). The Fabry-Perot resonator used is a single-mode fiber 20 cm long and has a comb of resonances 300 MHz apart, with a 3dB bandwidth of approximately 50 MHz. This frequency spacing is chosen because the minimum optical frequency spacing needed to prevent co-channel interference in the IF domain for 45 Mbits/s is 260 MHz.

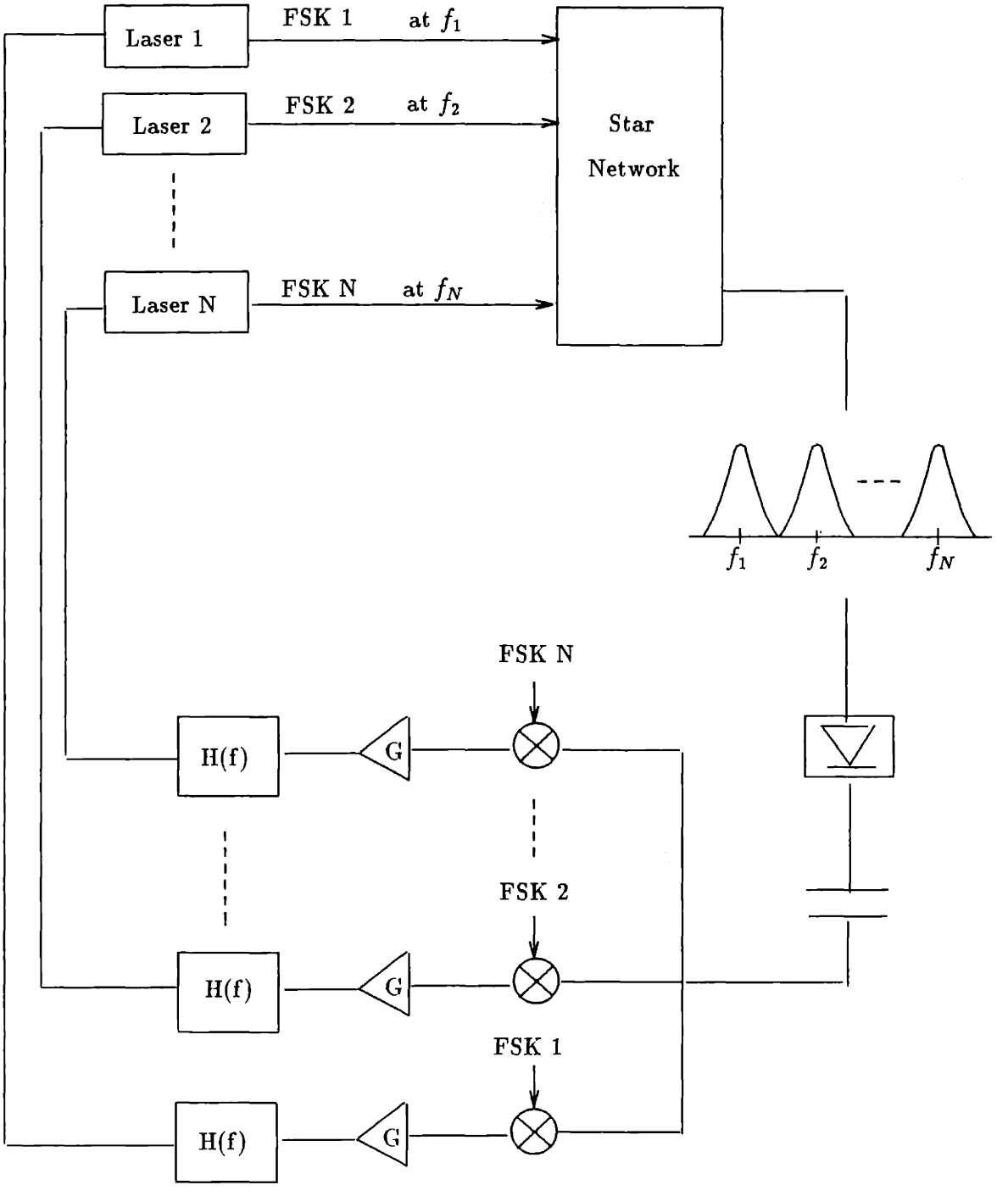

Figure 2.1: Frequency Stabilization Circuit

The error signal in this feedback loop is generated by the following manner. When the optical signal source drifts from its assigned frequency (one of the resonant frequencies of the Fabry-Perot), the Fabry-Perot will produce an optical intensity proportional to the drift. The photodiode then converts the optical intensity from the output of the Fabry-Perot to a baseband signal. The bit pattern in FSK is now a bit pattern in AM. The polarity of the AM bit stream signal is dependent on which side of the resonance the frequency drifted. After the Fabry-Perot and Photodetector, the DC signal (constant bias current to keep the lasers at the resonant frequencies) must be removed , since only the frequency deviation from resonance is of interest. Each user then multiplies the photocurrent bit pattern (whose amplitude is the error signal) by the FSK bit pattern to extract the error signal which is fed back to the laser as correction to lock the laser onto the designated Fabry-Perot resonance. Performance is deteriorated by the noise (the other user's bit streams are the most dominant) corrupting the error signal.

Experimental results showed that this frequency locking scheme is very robust. The FDM optical signals are heterodyned from the optical domain to the IF domain and monitored on a spectrum analyser. The three lasers remained locked to the selected resonant frequencies when the free-running laser frequency variation is up to ± 2.2 GHz. For larger tuning, the lasers would jump mode and onto other resonances [5].

Experimental results for another experiment using the same stabilization sheme, but with six lasers (that have better linewidth than the experiment with three lasers), were also good. The lasers used were multiple quantum well distributed Bragg reflector lasers (MQWDBR), transmitting around 1.53μm wavelength, and frequency tunable over 1,000 GHz, and having a narrow linewidth (2-4 MHz). They can be FSK-modulated up to a few hundred Mbits/s. The lasers in this FDM coherent optical network are multiplexed by a 16×16 optical-fibre star network. Since these monolithic frequency-tunable lasers are FSK modulated at 200 Mbit/s, the channel

spacing is 2.2 GHz (minimum possible spacing without adjacent channel interference). The channels are accessed by computer control. Glance showed that these six lasers were also stabilized well.

This stabilization technique can certainly work for one laser and separate feedback loops , each containing a Fabry-Perot can be implemented for each laser. Then the dominant user noise from the other lasers would not be present, there would be no need for the Low Pass Filter, and stabilization performance would undoubtedly improve. This technique would be just like the typical method described in the previous section. However, this scheme would have a problem in a FDM system, because the Fabry-Perot's resonant frequencies (which is used as a frequency discriminator and reference) will drift in time, with temperature, etc. Then the frequency channels of the users will collide into each other. Hence, the major advantage of Glance's stabilization system is that a single Fabry-Perot is used so the channel spacings between the users are controlled, preventing channel crossover. Another advantage of this system is that there are few components (only a Fabry-Perot Resonator, a photodiode, and simple electronics). The disadvantage of this stabilization scheme are that the optical sources must transmit from the same location. Glance has also developed a similar scheme for lasers transmitting from different locations. He uses a master Fabry-Perot to stabilize the other Fabry-Perot's in different regions [5].

It is intuitively clear that the Low Pass Filter is needed to filter out the user noise which is the dominant factor in degrading the stabilization performance. Right after the photodiode and before the correlator, each user gets the sum of every user's data stream scaled by their respective individual error signals of which each is only interested in extracting its own error signal, which it does so by correlating data streams. Clearly, the worst case is if all the user data streams are the same, then after correlation and filtering, each laser gets not only its own error signal, but the sum of all the other error signals as well. However, since the data streams are all independent, the above case is unlikely if we wait long enough to decorrelate.

The bandwidth of the filter must be smaller than the bit rate for the above reason. If the bandwidth of the filter is small, then the integration time is long, so decorrelation is good, and the user noise is filtered out well, but then the system will not be able to track the drift of the laser if the drift is too quick. On the other hand, if the bandwidth of the filter is large, then the filter is quick in time and the system can track the drift well, but the decorrelation time is small so cannot filter out the user noise well. Hence, there is a trade-off in the bandwidth of the filter design.

2.2 Fabry-Perot Resonator as Frequency Descriminator

The Fabry-Perot Interferometer has many applications such as being used as the resonator for lasers, as an optical filter, and as an optical spectrum analyzer. This device consists of two parallel partially transmitting and generally highly reflective mirrors that are spaced apart by a distance L. The important property of the Fabry-Perot is its frequency dependent transmission of power. The transmission characteristics are derived via computing the multiple reflections in the cavity.

Let E_0 be the incident electric field (with angle θ with respect to the mirror normal; for ease of explanation, let $\theta = 0$) of Figure 2.2. It is partially reflected with factor r_0 and partially transmitted with factor t_i. After a delay of length L, this wave is partially reflected with factor r_i and transmitted with t_0, resulting in T_1. Then, T_2 is the electric field resulting from two more reflections and delay of $2L$. The total transmitted field is the sum of all the transmitted fields $\sum_{i=1}^{\infty} T_i$. The measurement is a power density(irradiance, w/m^2), not electric field. This power density is related to the electric field by $H = \frac{EE^*}{2Z_0}$ where E is the electric field and Z_0 is the characteristic impedance of air (377Ω). The power transmitted per unit area is

$$P(f) = \frac{(1-R)^2}{(1-R)^2 + 4R\sin^2(\frac{2\pi nf}{cL})} \tag{2.1}$$

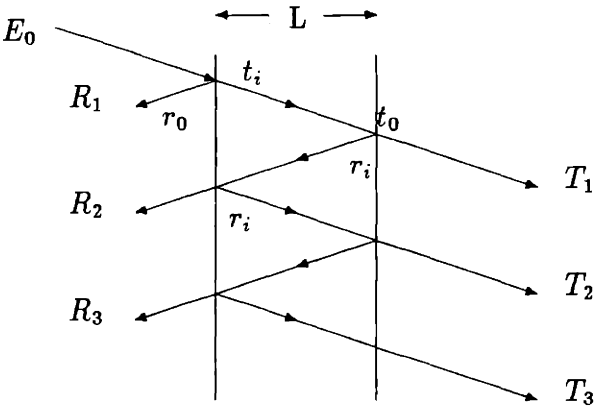

Figure 2.2: Fabry-Perot Interferometer

where $R = r_i^2 = r_0^2$ is the reflectivity of the mirrors (reflected power per unit incident power), f is optical frequency, c is the speed of light, and n is the refractive index of the resonant cavity. From Equation 2.1, the resonant frequencies (100% transmitted power, 0 reflected), f_m for integer $m > 0$, occurs when $\sin^2(\frac{2\pi nf}{cL}) = 0$. These transmission peaks are the resonant frequencies and are given by the equation (note that we have incorporated incident angle θ)

$$f_m = \frac{mc}{2nl\cos\theta} \tag{2.2}$$

The frequency separation of these resonant peaks is called the mode spacing or Free Spectral Range (FSR)

$$FSR = f_{m+1} - f_m = \frac{c}{2nl\cos\theta} \tag{2.3}$$

in terms of frequency and

$$FSR = \frac{\lambda^2}{2nl}\cos\theta \tag{2.4}$$

in terms of wavelength. The "full width at half-maximum" of the transmission peaks, call it $\delta_{1/2}$, can be calculated from Equation 2.1

$$\delta_{1/2} = \frac{(1-R)c}{2\pi\sqrt{R}nL\cos\theta} \tag{2.5}$$

and the finesse of the Fabry-Perot is defined as

$$Finesse = \frac{FSR}{\delta_{1/2}} = \frac{\pi\sqrt{R}}{1-R} \tag{2.6}$$

Figure 2.3 shows the Fabry-Perot transfer function for two different finesse. The higher the reflectivity, the higher the finesse, the sharper the frequency discrimination, the more expensive the device.

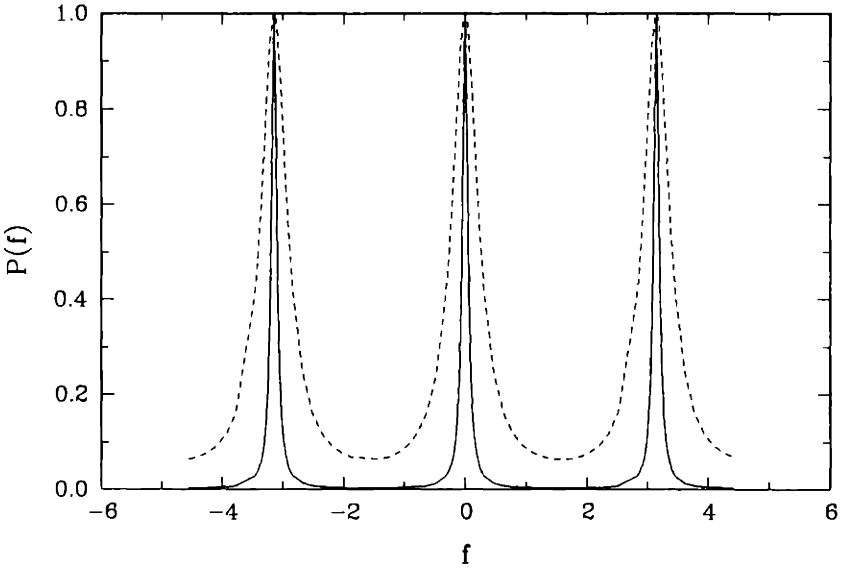

Figure 2.3: Fabry-Perot transfer function for $R = 0.9$ (solid) and $R = 0.6$ (broken)

The photodetector is a device that transfers optical energy (photons) to an electrical signal (current) for processing. There are two main types of semiconductor photodetectors: (1) The PIN photodiode is popular for data rates less than 100 Mbits/s, and (2) the APD (Avalanche photodiode) is popular for data rates greater than 1 Gbit/s. The quantum efficiency of the photodetector is defined to be the fraction of incident photons converted into carriers at the electrodes. There is a trade off between Quantum efficiency and speed. A high response time is paid by reduced sensitivity. Also, in the APD, the bandwidth decreases with increasing gain. When

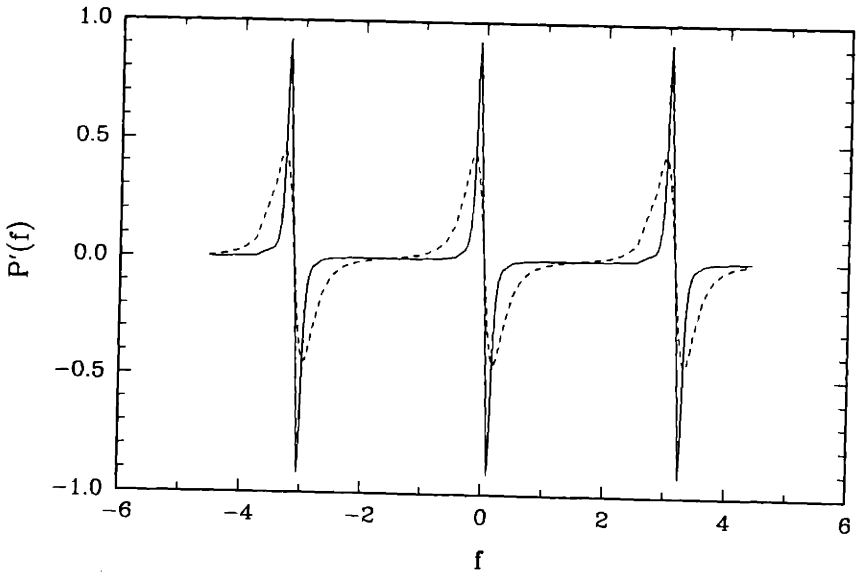

Figure 2.4: Frequency discrimination of the Fabry-Perot's in Figure 2.3

there is no light, both PIN and APD produce a small current due to thermal excitation of carriers. This is called "dark current" and represents background noise signal. In our model of the frequency discriminator, we assume the response time of the photodetector is immediate (i.e. the delay is negligible).

In the stabilization experiment, the laser frequencies are locked onto the resonant peaks, f_m, of the Fabry-Perot, call it the center frequencies. The FSK modulation frequencies, f_{m0}, f_{m1}, are equidistant from the center frequency. The error signal is obtained after demodulation. The frequency deviation in the laser is converted to amplitude variation in optical intensity. The frequency discrimination of the Fabry-Perot is approximately the first derivative of the power transfer function in Equation 2.1, which is linear within a range for each center frequency as shown in Figure 2.4; the locking range extends a bit beyond the linear range. For fixed FSR and modulation frequency distance $(f_{m0} - f_{m1})$, we see that a higher finesse results in a steeper slope (high gain) but smaller locking range. The bit rate will determine the minimum channel spacing and hence, the FSR, and the laser will determine FSK modulation spacing. Thus, the Fabry-Perot should be chosen such that the locking range is as

large as possible but the discriminator still linear. Assuming there is no laser intensity noise, this resulting loss in gain may affect the performance if the gain cannot be put back into the system (we shall see why in the next section).

The transfer functions for the feedback loop discriminator is as follows. Let C frequency/current be the transfer constant for the laser, D current/photons be the transfer constant for the photodiode, and B photons/frequency be the tranfer constant for the Fabry-Perot discriminator. Then, the total transfer function η for the open loop within the locking range is $\eta(f) = BCDf$, where f is the frequency deviation. Assume that $BCD = 1$ so that everything is normalized. If the physical parameters will not allow it, then assume we normalize it in the gain of the filter (which we are free to design). The frequency discriminator function is now linear with slope one.

2.3 Linearized Model and Assumptions

We assume there are N users on this FDM system and all the users are operating on the correct resonant freqeuncies. Although there is a locking range for the linear discriminator, we assume that it extends from negative infinity to positive infinity. The lasers may lose lock and jump modes, but we will not be concerned about that. The laser frequency noise which the stabilization system attempts to track is approximated to be white Gaussian noise. This is the random fluctuations from center frequency (optical domain) or random fluctuations from zero amplitude (after the photodetector). The criterion used to measure the frequency stabilization performance will be the MSE of the error signal. We will model the system by modelling the behavior from the standpoint of one laser.

Recall from the previous section that the total transfer constant of the cascade of all the individual devices (laser, photodiode, Fabry-Perot) is normalized to one. Hence the laser noise process in frequency is now converted to a random process in

amplitude with the same stochastic characterization.

The user noise in the system is the main contribution to system degradation and will dominate over system noise (such as shot noise, "dark current", background signal noise, etc.). The dominant noise from the other users is the current fluctuation caused by their modulation when they have a frequency offset. The user noise is seen right after the photodiode and it consists of the sum of the other user's bit streams multiplied by their individual error signals. In reality, the locking range is finite (although we modelled the linear region of the frequency discriminator as extending to infinity), so the error signal amplitude is in fact bounded. Hence, it is reasonable to assume that all the rest of the user frequency drift with constant offset equal to the locking range, call it L. That is, all users put on the channel the worst noise. The amplitude of their bit streams is L. Since we have two degrees of freedom in the transfer constants described above, we can assume D, the transfer constant for the photodiode to be $1/L$, so that the error amplitudes of the other user bits streams are all one.

The stabilization system can be modelled as in Figure 2.5 where $x_1(t)$ is the laser frequency noise with power spectral density $S_{xx}(f)$, $d_1(t)$ is the data stream of user one, $u(t)$ is the sum of all other user's data streams, $v(t)$ is the system noise, and $H(f)$ is the filter.

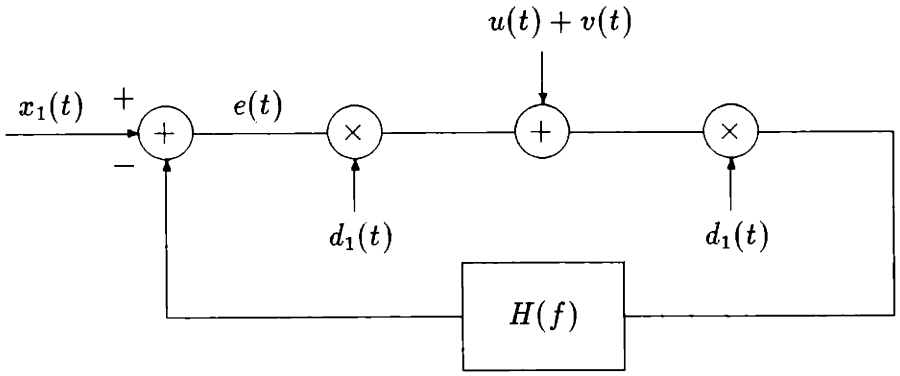

Figure 2.5: Model I of Stabilization System

Each user i in the system is modulating with independent random NRZ (non return to zero) data stream $d_i(t)$ and bit time T, which can be described by

$$d_i(t) = \sum_{n=-\infty}^{\infty} I_i(n)p(t - nT + \tau_i) \tag{2.7}$$

where for each i

$$I(n) = \begin{cases} 1 & p = \frac{1}{2} \\ -1 & p = \frac{1}{2} \end{cases}$$

and

$$p(t) = \begin{cases} 1 & 0 < t < T \\ 0 & \text{otherwise} \end{cases}$$

To make $d_i(t)$ WSS, let τ_i randomize the start time where $P_{\tau_i}(\tau)$ be uniformly distributed over the interval $[0, T]$. The user noise in the system is the sum of all the other users bit streams and denoted by

$$u(t) = \sum_{i=2}^{N} \sum_{n=-\infty}^{\infty} I_i(t)p(t - nT + \tau_i) \tag{2.8}$$

Noticing that $d_i(t)d_i(t) = 1$, the model in Figure 2.5 can be reduced to the model in Figure 2.6.

Now the noise from the other users, call it $n(t)$, becomes

$$n(t) = d_1(t)u(t) = \sum_{i=2}^{N} \sum_{n=-\infty}^{\infty} I_i(n)p(t - nT + \tau_i)I_1(n)p(t - nT + \tau_1) \tag{2.9}$$

The closed loop transfer functions of Figure 2.6 are as follows

$$\begin{aligned} Y(f) &= \frac{H(f)}{1 + H(f)}[X(f) + N(f)] \\ E(f) &= \frac{1}{1 + H(f)}[X(f) + N(f)H(f)] \end{aligned}$$

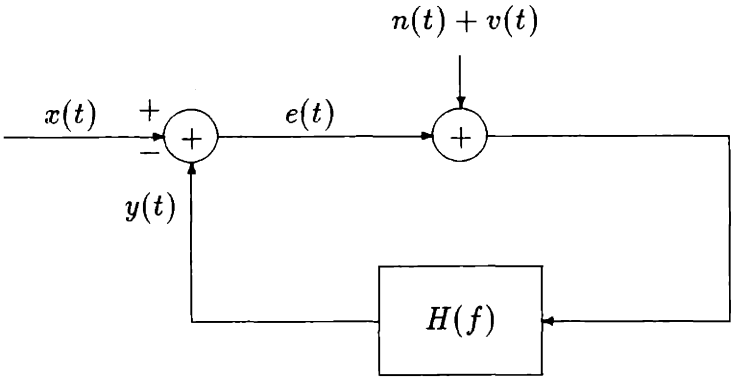

Figure 2.6: Reduced System Model I

and the Power Spectral Densities are

$$\begin{aligned} S_{yy}(f) &= \left|\frac{H(f)}{1+H(f)}\right|^2 [S_{xx}(f) + S_{nn}(f)] \\ S_{ee}(f) &= \left|\frac{1}{1+H(f)}\right|^2 \left[S_{xx}(f) + |H(f)|^2 S_{nn}(f)\right] \end{aligned} \tag{2.10}$$

As mentioned earlier, the criterion used to evaluate performance is mean squared error (MSE).

$$MSE = E[e(t)^2] = \int_{-\infty}^{\infty} S_{ee}(f)df \tag{2.11}$$

To minimize $E[e(t)^2]$, the MSE, for causal $h(t)$, Wiener Filtering methods will be employed. The noncausal $h(t)$ will provide a lower bound on the MSE. For a noncausal optimal filter, we minimize equation(2.11) by minimizing the integrand.

As mentioned earlier, we normalized the product of all the transfer constants in the stabilization loop to one by assuming we can take care of it in the gain of the filter, $H(f)$. If, due to physical limitations, the normalization cannot be achieved, then the filter will be suboptimal. Let that suboptimal filter be $G(f) = kH(f)$ where

$k < 1$ and $H(f)$ is the optimal filter. Then the power spectral density of the error signal will be

$$S_{ee}(f) = \left|\frac{1}{1+kH(f)}\right|^2 S_{xx}(f) + \left|\frac{H(f)}{\frac{1}{k}+H(f)}\right|^2 S_{nn}(f) \tag{2.12}$$

and the suboptimal MSE can be evaluated.

2.4 Noise

Besides the system noise v(t), there are three types if user noises $n_1(t), n_2(t), n_3(t)$ whose statistics depend on the model we use.

2.4.1 System Noise

The "dark current" of the photodiode, shot noise, electrical noise, and any other physical noise will be lumped together and modelled as white Gaussian noise. We will refer to these noises as system noise, $v(t)$, with spectral height $S_{vv}(f) = V$.

2.4.2 Synchronous Users

The users are synchronous when they all have the same random start time $\tau_i = \tau_1 \ \forall i$. Let's define $n_1(t)$ as the synchronous user noise. Then equation(2.9) reduces to

$$n_1(t) = \sum_{i=2}^{N} \sum_{n=-\infty}^{\infty} J_i(n) p(t - nT + \tau) \tag{2.13}$$

where

$$J_i(n) = I_1(n) I_i(n) = I(n) \tag{2.14}$$

Since all the bit streams are independent, the autocorrelation function is the autocorrelation function of one bit stream multiplied by the number of bit streams.

$$E\left[n_1(t+\tau) n_1(t)\right] = (N-1) E\left[d(t+\tau) d(t)\right] \tag{2.15}$$

$$R_{n_1 n_1}(\tau) = (N-1)[1 - \frac{|t|}{T}] \tag{2.16}$$

The Power Spectral Density is the Fourier Transform of $R_{n_1 n_1}(\tau)$ which in this case is the convolution of two square pulses. Hence, $S_{n_1 n_1}(f)$ is the sinc function squared, shown below in figure 2.7

$$S_{n_1 n_1}(f) = (N-1)T\left[\frac{sin\pi fT}{\pi fT}\right]^2 \tag{2.17}$$

The Power Spectral Density can also be represented by the Bilateral Laplace Transform of $R_{n_1 n_1}(\tau)$ which is

$$S_{n_1 n_1}(s) = (N-1)\left[\frac{e^{sT/2} - e^{-sT/2}}{s}\right]^2 \tag{2.18}$$

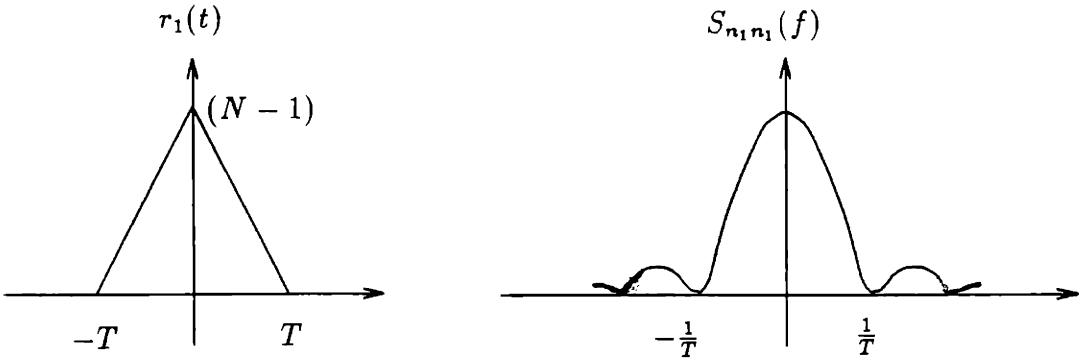

Figure 2.7: Synchronous Autocorrelation Function and corresponding Power Spectral Density

2.4.3 Asynchronous Users

The users are asynchronous when their random start times are all independent. Let's define $n_2(t)$ as the asynchronous noise.

$$n_2(t) = s_1(t) \cdot \sum_{i=1}^{N} s_i(t) \tag{2.19}$$

Again, the bit streams are independent, so the autocorrelation function is just the sum of the individual autocorrelation functions.

$$\begin{aligned} E\left[n_2(t+\tau)n_2(t)\right] &= (N-1)E\left[s_1(t+\tau)s_2(t+\tau)s_1(t)s_2(t)\right] \\ &= (N-1)R_{n_1n_1}(\tau)^2 \\ &= (N-1)\left[1-\frac{|t|}{T}\right]^2 \end{aligned} \tag{2.20}$$

with corresponding Power Spectral Density

$$\begin{aligned} S_{n_2n_2}(f) &= \int_{-\infty}^{\infty} R_{n_2n_2}(\tau)e^{-j2\pi ft}dt \\ &= (N-1)\int_0^T \left(1-\frac{t}{T}\right)^2 2cos(2\pi ft)dt \\ &= \frac{(N-1)T}{(\pi fT)^2}\left[1-\frac{sin2\pi fT}{2\pi fT}\right] \end{aligned} \tag{2.21}$$

and Bilateral Laplace Transform

$$S_{n_2n_2}(s) = \frac{4(N-1)}{s^2T}\left[\frac{e^{sT}-e^{-sT}}{2sT}-1\right] \tag{2.22}$$

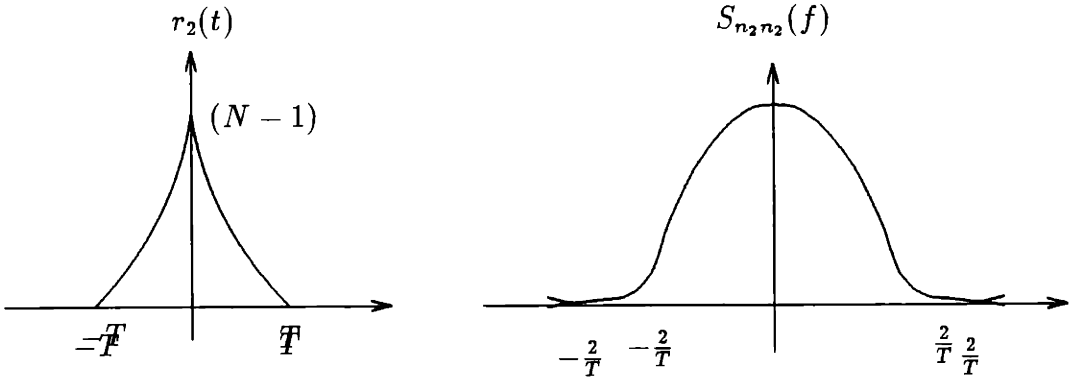

Figure 2.8: Asynchronous Autocorrelation Function and corresponding Power Spectral Density

2.4.4 Random Telegraph Signal

The user's bit streams modulation is dependent on a Poisson count. Let the bit streams be the stochastic process $z(t) = a \cdot f\left[n(o,t)\right]$ where

$$p\left[n(0,t)=k\right]=\frac{e^{-\lambda t}(\lambda t)^k}{k!} \tag{2.23}$$

$$f\left[n(0,t)=k\right]=\begin{cases} 1 & \text{if } n(0,t) \text{ is odd} \\ -1 & \text{if } n(0,t) \text{ is even} \end{cases}$$

$$a=\begin{cases} 1 & p=\frac{1}{2} \\ -1 & p=\frac{1}{2} \end{cases}$$

The bit sequence is such that as soon as there is an arrival from the Poisson process, the bit stream changes polarity ($1 \rightarrow -1$ or $-1 \rightarrow 1$) at the time of the arrival. The random variable a is to randomize the starting bit at $t = 0$ so that the process is WSS. Then, the autocorrelation function is calculated to be

$$R_{zz}(t)=e^{-2\lambda|\tau|} \tag{2.24}$$

and corresponding Power Spectral Density

$$S_{zz}(f)=\frac{\lambda}{\lambda^2+(\pi f)^2} \tag{2.25}$$

We are interested in the RTW example because its exponential autocorrelation function can approximate the user synchronous and asynchronous autocorrelation functions. This approximation is useful because the Power Spectral Density of the RTW is a rational function (whereas the Power Spectral Density of the synchronous and asynchronous user noises are not), and will allow us to find the optimal filter easily in closed form. Physically, we can view the RTW process in our bit sequence as follows. Due to independence of nonoverlapping time intervals of the Poisson process and that a bit time T is very small, P[arrival in (0,T)] = P[bit change in (0,T)] implies that $\lambda T = \frac{1}{2}$. Alternatively, let $t = nT$ where n is a large integer, we expect E[# arrivals in (0,t)] = E[# bit changes in (0,t)] which implies $\lambda nT = (\frac{1}{2})n$, giving $\lambda = \frac{1}{2T}$.

From Equation 2.9, the noise in the system is

$$n_3(t) = z_1(t) \cdot \sum_{i=2}^{\infty} z_i(t) \tag{2.26}$$

which is a sum of $n-1$ independent random telegraph waves. For the synchronous case approximation, the Poisson rate is the same, but for the asynchronous case the Poisson rate is doubled (the sum of independent Poisson processes is a Poisson process with the rates summed). We will only consider the asynchronous case since it better models reality. So the autocorrelation function is

$$R_{n_3 n_3}(\tau) = (N-1)e^{-4\lambda|\tau|} = (N-1)e^{\frac{2}{T}|\tau|} \tag{2.27}$$

with corresponding Power Spectral Density

$$S_{n_3 n_3}(f) = (N-1)\frac{\frac{1}{T}}{(\frac{1}{T})^2 + (\pi f)^2} \tag{2.28}$$

and Bilateral Laplace Transform

$$S_{n_3 n_3}(s) = (N-1)\frac{\frac{4}{T}}{(\frac{2}{T})^2 - s^2} \tag{2.29}$$

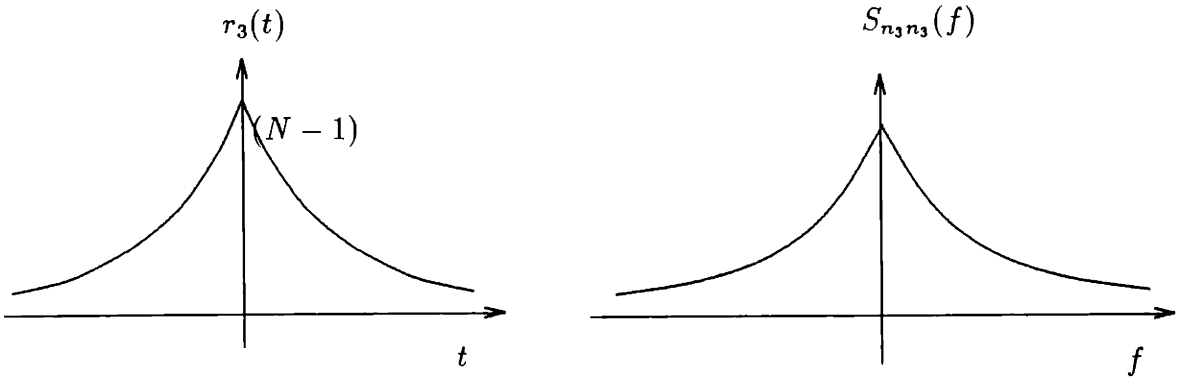

Figure 2.9: Random Telegraph Wave Autocorrelation Function and corresponding Power Spectral Density

From here on, we use the notation $S_{nn}(f)$ to describe a generic user noise spectral density and $S(f)$ is the Power Spectral Density of a generic single bit stream (binary transmission). Then, $S_{nn}(f) = (N-1) \cdot S(f) = S_{n_i n_i}(f)$ for $i = 1, 2, 3$.

Chapter 3

Optimum Filter

3.1 Noncausal Filter

We seek to find the filter $H(f)$ which minimizes the MSE, given no causality constraints. From the previous section, recall

$$E[e(t)^2] = \int_{-\infty}^{\infty} \left| \frac{1}{1+H(f)} \right|^2 \left[S_{xx}(f) + |H(f)|^2 S_{nn}(f) \right] df \tag{3.1}$$

Examining equation(2.10), we see that since $S_{xx}(f)$ is a constant (white noise component), $H(f)$ must approach ∞ as $f \uparrow$ to produce a finite variance. In fact, $H(f)$ must increase at least as fast as f, which means $h(t)$ must contain at least a differentiator. Furthermore, for finite MSE, $n(t)$ must have finite power.

In general, $H(f)$ is complex, but since $S_{xx}(f) \geq 0$ and $S_{nn}(f) \geq 0$, $\forall f$, the integrand is minimized when $H(f)$ is real. This is true, because for any $|H(f)|$ in the complex plane, $|\frac{1}{1+H(f)}|$ is minimized when $|H(f)| = H(f)$. Hence, equation (3.1) can be reduced to

$$E[e(t)^2] = \int_{-\infty}^{\infty} \left(\frac{1}{1+H(f)} \right)^2 \left[S_{xx}(f) + H(f)^2 S_{nn}(f) \right] df \tag{3.2}$$

To minimize the integrand, call it I, in equation(3.1), let $h = H(f)$, then solve for h such that $\frac{d}{dh} I = 0$ and checking $\frac{d^2}{dh^2} I > 0$ shows that indeed the optimal causal filter is

$$H(f) = \frac{S_{xx}(f)}{S_{nn}(f)} \tag{3.3}$$

Since spectral densities are even, $H(f)$ is also even. Thus, $h(t)$ is real and even. For the noncausal filter, the MSE becomes

$$E[e(t)^2] = \int_{-\infty}^{\infty} \frac{S_{xx}(f) \cdot S_{nn}(f)}{S_{xx}(f) + S_{nn}(f)} df \tag{3.4}$$

Let the integrand in Equation 3.4 be J, then notice that

$$\frac{1}{J} = \frac{1}{S_{xx}(f)} + \frac{1}{S_{nn}(f)} \tag{3.5}$$

After a change of variables, where $u_1 = \pi f T$ and $u_2 = 2\pi f T$ for synchronous and asynchronous repectively, and the integration is now over u_i, $i = 1, 2$,

$$\frac{1}{J} = i\,\pi\,T \left[\frac{1}{A} + \frac{1}{(N-1)S(u_i) + V} \right] \tag{3.6}$$

The effect of the spectral height of the laser, the number of users N, and the bit stream T on the MSE can be seen. The different noise Power Spectral Density $S_{nn}(f)$ is given in equations(2.17,2.21, 2.28). If the spectral height of the laser noise A, the number of users N, or the system noise V increases, then $\frac{1}{J}$ decreases, and the MSE increases. System performance degrades as we would expect. If the bit time T increases, the MSE also decreases. This is reasonable, since the price paid for a better system is a lower bit rate. On the other hand, this fact is against our intuition about the system, as we believed that a quicker bit rate will decorrelate the binary bit streams quicker, resulting in better system performance.

In the results section, we numerically integrate Equation 3.4 to obtain the MSE and discuss the results in further detail.

3.2 Causal Filter

3.2.1 Basic Wiener Filtering Theory

The Wiener filter is the CT causal filter that provides the LLSE of a random process from a random process observation. Let $x(t)$ be the CT process to be estimated, $n(t)$

the additive noise, $\hat{x}(t)$ the estimate, and $\{y(\tau) : T_i < \tau < T_f\}$ the observed random process. For the causal Wiener filter, $\{y(\tau) : -\infty < \tau < t\}$. Their mean $E[x(t)]$, $E[y(t)]$, autocovariance functions $R_{xx}(\tau), R_{yy}(\tau)$, and cross-covariance $R_{xy}(\tau)$ must be known. The linear, time-varying filter $h(t,\tau)$ which minimizes the mean squared error MSE $= E\left[(x(t) - \hat{x}(t))^2\right]$ is the Wiener filter. The general model is shown in Figure 3.1.

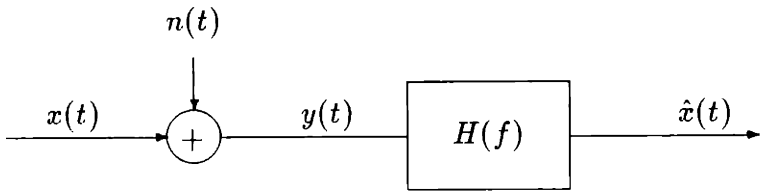

Figure 3.1: Wiener Filter Problem

$$\hat{x}(t) = \int_{T_i}^{T_f} h(t,\tau)y(\tau)d\tau \tag{3.7}$$

The optimal causal estimate is the one whose estimation error is orthogonal to the past observations.

$$E[(x(t) - \hat{x}(t))y(\tau)] = R_{xy}(t,\tau) - \int_{T_i}^{T_f} h(t,\sigma)R_{yy}(\sigma,\tau)d\sigma = 0 \tag{3.8}$$

which gives the Wiener-Hopf equation

$$R_{xy}(t,\tau) = \int_{T_i}^{T_f} h(t,\sigma)R_{yy}(\sigma,\tau)d\sigma \qquad T_i < \tau < T_f \tag{3.9}$$

that the LLSE filter must be the solution to.

The random observation process are WSS and JWSS and since $h(t,\sigma)$ is causal and the equation is satisfied for arbitrary time t, the above equation becomes

$$R_{xy}(t) = \int_0^{\infty} h(\tau)R_{yy}(t-\tau)d\tau \qquad 0 < t < \infty \tag{3.10}$$

If the observation process $y(t)$ is 0-mean WSS unit-strength white noise, then

$$h(t) = R_{xy}(t)u_{-1}(t) \tag{3.11}$$

which is the causal part of the cross-covariance function.

If $y(t)$ is otherwise, then we can decompose the problem by whitening the observation by a whitening filter $W(s)$ which is both causal and causally invertible. For convenience, let us whiten to unit spectral height.

$$S_{yy}(s)W(s)W(-s) = 1 = S_{vv}(s) \tag{3.12}$$

That is, the time function corresponding to $W(s)$ and $1/W(s)$ must be causal. Then, $W(-s)$ must be anticausal. For example, if $S_{yy}(s)$ is rational, then $W(s)$ must contain both poles and zeros in the Left Half Plane. It is intuitively clear that if prepossessing is causally reversible, then there is no performance degradation of the system. In other words, if we are unable to undo the processing then we have lost information and the resulting filter is not optimal. The reversibility proof is as follows. Suppose that there are two systems shown in Figure 3.2. If G^+ is causal, then system 1 is no worse than system 2. If $\frac{1}{G^+}$ is causal, then system 2 is no worse than system 1.

Then we find the Wiener filter $G(s)$based on the white noise and the overall filter by the cascade of the filters, $H(s) = G(s)W(s)$ as in Figure 3.3 below.

Now, $G(s) = \{S_{xv}(s)\}_+ = \{S_{xy}(s)W(-s)\}_+$ where the notation $\{S_{xv}(s)\}_+$ is the Bilateral Laplace Transform (BLT) of $R_{xv}(t)u_{-1}(t)$. Recall that

$$R_{xy}(\tau) = E\left[x(t+\tau)y(t)\right] \tag{3.13}$$

$$S_{xy}(s) = \int_{-\infty}^{\infty} R_{xy}(\tau)e^{-s\tau}d\tau = S_{xx}(s)H(-s) \tag{3.14}$$

Similarily,

$$S_{yx}(s) = S_{xx}(s)H(s) \tag{3.15}$$

The causal Wiener filter which minimizes the MSE between the observation process and estimate is:

$$H(s) = W(s) \cdot \{S_{xy}(s) \cdot W(-s)\}_+ \tag{3.16}$$

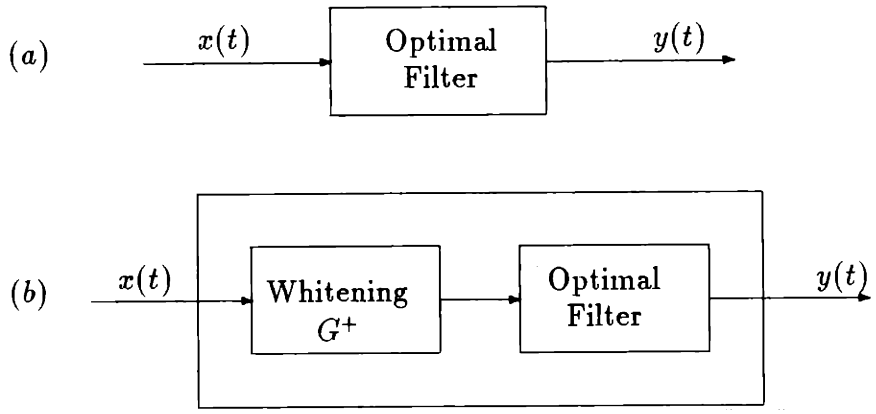

Figure 3.2: Reversibility Proof: (a) System 1 (b) System 2

3.2.2 Model for Causal Filter

We can transform the problem to a Wiener filtering problem as follows. Let $y(t)$ be the observation process and $x(t)$ the process to be estimated. Since $x(t)$ and $n(t)$ are independent, they are uncorrelated, $E[x(t)n(t)] = 0$. We will derive the causal Wiener filter via two approaches. For our system model in Figure 3.4, the following spectral densities are

$$S_{xx}(f) = A \tag{3.17}$$

$$S_{yy}(f) = \left|\frac{1}{1+H(f)}\right|^2 [S_{xx}(f) + S_{nn}(f)] \tag{3.18}$$

$$S_{xy}(f) = S_{xx}(f)H(f)^* = \frac{1}{1+H(f)^*} S_{xx}(f) \tag{3.19}$$

The optimal causal filter from Equation 3.16 is then

$$H(f) = [1 + H(f)]W(f)\left\{\frac{S_{xx}(f)}{1+H(f)^*}[1 + H(f)^*]\,W(f)^*\right\}_+ \tag{3.20}$$

where $x(t)$ is a 0-mean white noise component with spectral height A, and $W(f)W(f)^*[S_{xx}(f)+S_{nn}(f) = 1$ with $W(f)$ causal and causally invertible. Solving for the optimal filter,

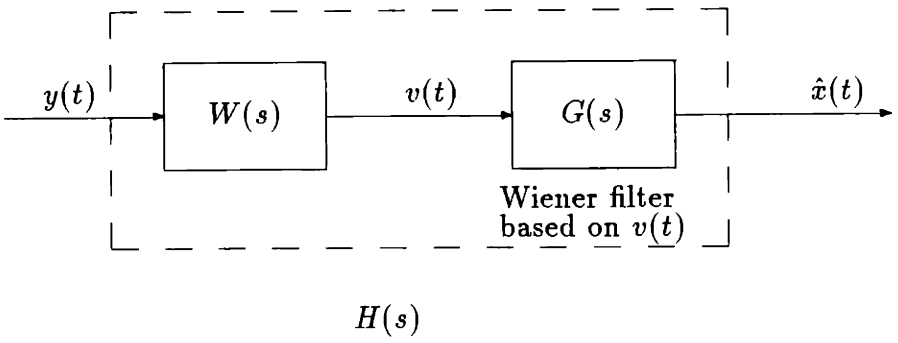

Figure 3.3: Wiener filter for Colored Noise Observations

$$H(f) = \frac{W(f)\{S_{xx}(f) \cdot W(f)^*\}_+}{1 - W(f)\{S_{xx}(f) \cdot W(f)^*\}_+} \tag{3.21}$$

Alternatively, if we use the idea of lumping the closed loop system function as in Figure 3.5, then

$$G(f) = \frac{H(f)}{1 + H(f)} \quad \text{and} \quad H(f) = \frac{G(f)}{1 - G(f)} \tag{3.22}$$

$$S_{xx}(f) = A \tag{3.23}$$

$$S_{yy}(f) = S_{xx}(f) + S_{nn}(f) \tag{3.24}$$

$$S_{xy}(f) = S_{xx}(f) \tag{3.25}$$

Then, $G(f)$ is the Wiener filter

$$G(f) = W(f)\ \{S_{xx}(f) \cdot W(f)^*\}_+ \tag{3.26}$$

and solving for the optimal filter $H(f)$ by substituting Equation 3.22

$$H(f) = \frac{W(f)\{S_{xx}(f) \cdot W(f)^*\}_+}{1 - W(f)\{S_{xx}(f) \cdot W(f)^*\}_+} \tag{3.27}$$

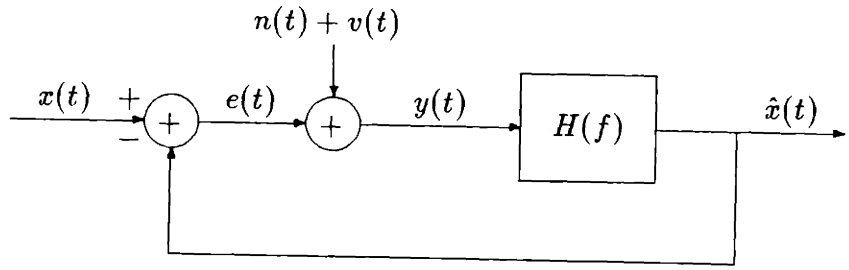

Figure 3.4: System Model I

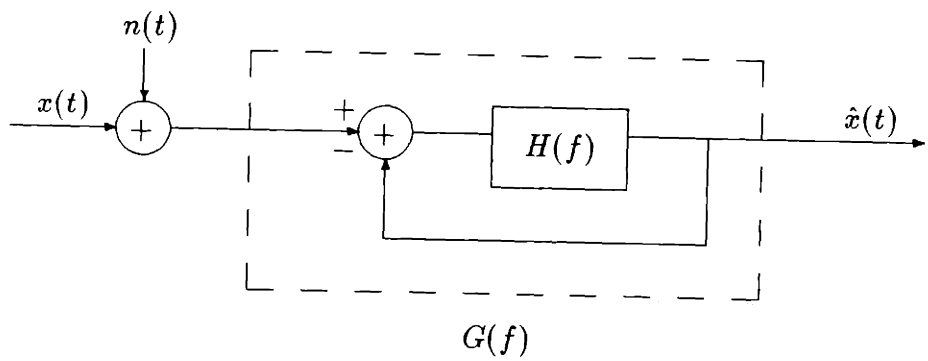

Figure 3.5: Model Reduction for Causal Filter

we get what was obtained previously.

Clearly, if $H(f)$ is causal, then $G(f)$ is causal. By the formulation of the problem, we are solving $H(f)$ is terms of $G(f)$, and hence, we are concerned about the causality of $H(f)$. If $G(f)$ is causal, then $H(f)$ is also causal. This fact is evident in Equation 3.22 where the transfer function $H(f)$ is the enclosed feedback system of Figure 3.5 where $G(f)$ and $H(f)$ are interchanged and the feedback is changed from negative to positive.

The optimal filter of Equation 3.27 can be further reduced. Within the brackets of the above equation is the positive time component of $A\delta(t) * w(-t)$. Since $w(-t)$ is anti-causal, it must have a delta function at the origin or else the optimal causal

filter is $H(f) = 0, \forall f$. That is, the mean is always guessed. We show in the next section that the whitening filter $W(f)$ does indeed have a delta function at the origin. Hence, the optimal filter can be reduced to equation(3.28) for a constant C. In a later section we show this $C = \frac{1}{\sqrt{A}}$.

$$H(f) = \frac{W(f) \cdot C}{1 - W(f) \cdot C} \tag{3.28}$$

3.2.3 Whitening Filter-Frequency Domain

Since power spectral densities are real and even, all poles and zeros in the complex plane are reflected about the real and imaginary axis, i.e., they have quadruple symmetry. Hence, if the function to whiten, $S_{yy}(s)$, were rational, the whitening filter could be found by spectral factorization. Since $W(s)W(-s)S_{yy}(s) = 1$, then $W(s)$ just contains all the pole and zeros of $S_{yy}(s)$ in the LHP. The whitening filter can be easily found for the random telegraph wave user noise, $S_{n_3 n_3}(s)$

If $S_{yy}(s)$ were not polynomial as in the cases for $S_{n_1 n_1}(s)$ and $S_{n_2 n_2}(s)$, the whitening filter is very difficult to find. Note that since $S_{nn}(f)$ is stable, the ROC includes the jw-axis, so $S_{nn}(s)$ is the complex extension of $S_{nn}(f)$ where $s = j2\pi f$. The magnitude of the whitening filter is $|W(f)| = \sqrt{1 + S_{nn}(f)}$, and all that is needed is to find $\angle W(f)$ such that $w(t)$ is causal. This angle exists for both user Spectral Densities by the Paley-Wiener Theorem which states that for any square-integrable function $|H(f)|$ that satisfies

$$\int_{-\infty}^{\infty} \frac{|\ln |H(f)||}{1 + f^2} df < \infty \tag{3.29}$$

there exists an $\angle H(f)$ such that $|H(f)| e^{j\angle H(f)}$ is the Fourier Transform of a causal $h(t)$. The theorem also states that if $h(t)$ is square-integrable and causal, then equation(3.29) is satisfied. Note that there are many factorizations where $S_{yy}(s) = Y(s)Y(-s)$, but $y(t)$ is not causal.

An attempt using the spectral factorization method on the nonpolynomial func-

tions was made. For both observations, $S_{yy}(s)$ contains no poles, but may contain zeros. If so, an approximation can be made by just capturing the zeros close to the origin, and the whitening filter will have as roots the zeros in the LHP. The roots far from the real axis correspond to high frequency components which is of lesser interest, since it is the low frequency components that are degrading the communication system. The roots (in LHP) far from the imaginary axis correspond to signals that decay quickly in time, so also have lesser effect. For the synchronous user case,

$$S_{yy}(s) = 1 + \frac{1}{s^2}[1 - e^{-sT}][1 - e^{sT}] = 1 + \frac{e^{sT/2} - e^{-sT/2}}{s^2} \tag{3.30}$$

and we wish to find its roots. Letting $s = \alpha$ we see there are no roots on the real axis since there is no real α that satisfies the equation $(e^{\alpha T/2} - e^{-\alpha T/2})^2 = -\alpha^2$. Letting $s = j\omega$, we also see there are also no roots on the imaginary axis, since $(e^{j\omega T/2} - e^{-j\omega T/2})^2 = \omega^2$ is also $\sin^2(\omega T/2) + \left(\frac{\omega}{2}\right) = 0$, and no real ω satisfies the equation. A computer program was generated to find the roots of $S_{yy}(s)$ and found that there was an infinite number of roots whose imaginary components were spaced at periodic intervals apart. The whitening filter $W(s) = (s-z_1)^{-1}(s-\overline{z}_1)^{-1}(s-z_2)^{-1}(s-\overline{z}_2)^{-1}\ldots$ is a rational function approximation. However, since $w(t)$ does not contain an impulse function at the origin, the optimal causal filter is zero as shown previously. Hence, this approximation is no good.

3.2.4 Whitening Filter-Time Domain

There are no general methods to find the whitening filter for nonpolynomial spectral densities, so we will try some time domain techniques. Suppose $r(t)$ is the function to be whitened. If a causal $y(t)$ with a causal inverse can be found such that $y(t)*y(-t) = r(t)$, then $w(t)$, the causal inverse of $y(t)$ (i.e. $w(t) * y(t) = \delta(t)$) is the whitening filter.

For example, suppose we are looking for a whitening filter to the triangle autocorrelation function in figure(3.6). Then we notice that $y(t) = 1, 0 < t < T$, and zero elsewhere convolved with $y(-t)$ will result in $r(t)$. The causal inverse to $y(t)$ can be seen

by inspection in the time domain as an infinite differentiator, $w(t) = \sum_{n=0}^{\infty} \dot{\delta}(t - nT)$, in figure(3.7). The inverse can also be obtained from the frequency domain where

$$W(s) = \frac{1}{Y(s)} = s(1 + e^{-sT} + e^{-2sT} + e^{-3sT} + \cdots) \tag{3.31}$$

and inverse transform to a causal $w(t)$. There is also the anti-causal inverse, call it $w'(t) = -\sum_{n=-\infty}^{-1} \dot{\delta}(t - nT)$ by inspection or from inverse transforming

$$W(s) = \frac{1}{Y(s)} = -e^{sT}(1 + e^{sT} + e^{2sT} + e^{3sT} + \cdots) \tag{3.32}$$

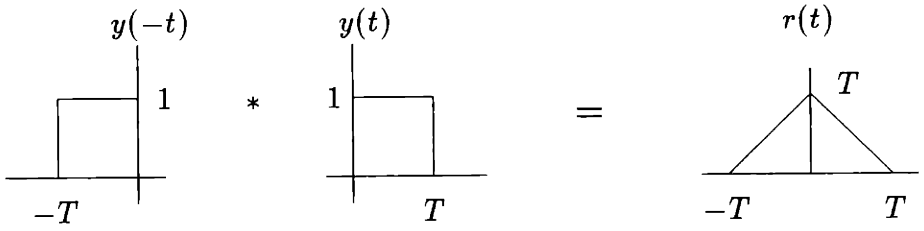

Figure 3.6: Triangular Autocorrelation Function r(t)

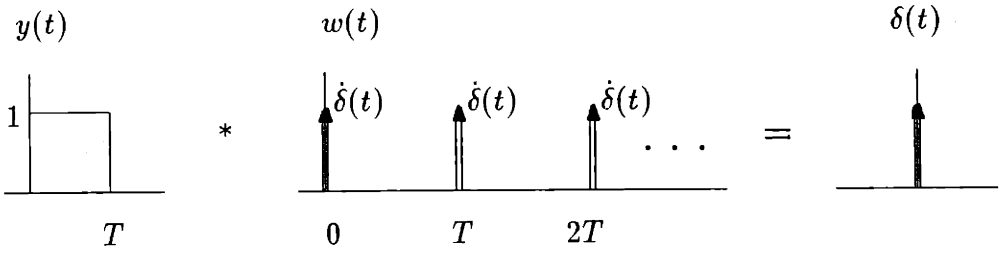

Figure 3.7: Causal Inverse to Square Pulse and Whitening Filter to r(t)

The nonpolynomial functions that need to be whitened are the user synchronous and asynchronous spectrums plus the spectral height of the laser shown in figure 3.8 below. Given that both functions have impulse function at the origin, we know that the causal part $y(t)$ must contain exactly one impulse funtion. There cannot be a

finite number of impulse functions in $y(t)$, because the resulting convolution with $y(-t)$ would produce a train of impulse functions. An infinite number of impulse functions in $y(t)$ is also impossible. The proof is as follows:

We show that for any $T > 0$ and $a_n \in \Re$, the only solution to

$$\sum_{n=0}^{\infty} a_n \delta(t - nT) * \sum_{n=-\infty}^{0} a_n \delta(t + nT) = \delta(t) \tag{3.33}$$

is $\pm\delta(t - T)\ \forall T \in \Re$. From equation(3.33) the conditions that must be satisfied are $\sum_{n=0}^{\infty} a_n^2 = 1$ and

$$\begin{bmatrix} a_0 \\ a_1 \\ a_2 \\ \vdots \end{bmatrix}^T \begin{bmatrix} a_0 & a_1 & a_2 & \cdots \\ a_1 & a_2 & a_3 & \cdots \\ a_2 & a_3 & a_4 & \cdots \\ \vdots & \vdots & \vdots & \ddots \end{bmatrix} = \begin{bmatrix} 1 \\ 0 \\ 0 \\ \vdots \end{bmatrix}^T \tag{3.34}$$

Suppose $[a_0\ a_1\ a_2\ \cdots]$ is a solution. Let $S_0 = [a_0\ a_1\ a_2\ \cdots]$, $S_1 = [0\ a_0\ a_1\ \cdots]$, $S_2 = [0\,0\,a_0\ \cdots]$, and so forth, where $a_0 \neq 0$. If $a_0 = 0$, then shift the whole sequence until a_0 is the first nonzero element in the sequence.

Equation 3.34 implies that the S_i are orthonormal. If they are a complete and orthonormal basis for ℓ^2 where $\ell^2(\Re)$ is the set of all sequences such that $\sum_{i=0}^{\infty} a_i^2 < \infty$, then any such sequence $f = \sum_{i=0}^{\infty} \langle f, S_i \rangle S_i$. Let $f = e_0^T$, where $e_0 = [1\ 0\ 0\ \cdots]^T$. Then, $e_0^T = \sum_{i=0}^{\infty} \langle e_0^T, S_i \rangle S_i = \langle e_0^T, S_0 \rangle S_0 = a_0 S_0$. This implies that $[1\ 0\ 0\ \cdots] = [a_0^2\ a_0a_1\ a_0a_2 \cdots]$. Hence, $a_0 = \pm 1$ and $a_i = 0$ for $i \neq 0$.

All we have left to do is show that the S_i's are complete. Because e_i are complete, if e_i can be written as a linear combination of S_i, then S_i are complete. We only need to show this is true for e_0, since the rest of the e_i are a shifted version of e_0, or we

can show it for all e_i. Now, S_i can be written as a function of e_i

$$\begin{bmatrix} S_0 \\ S_1 \\ S_2 \\ \vdots \end{bmatrix} = \begin{bmatrix} a_0 & a_1 & a_2 & \cdots \\ 0 & a_0 & a_1 & \cdots \\ 0 & 0 & a_0 & \cdots \\ \vdots & \vdots & \vdots & \ddots \end{bmatrix} \begin{bmatrix} e_0 \\ e_1 \\ e_2 \\ \vdots \end{bmatrix}^T \tag{3.35}$$

It is clear by the structure of the infinite dimension matrix that the rows are all independent. Let's represent Equation 3.35 by the Matrix multiplication $S = MI$. If we can find the inverse to the infinite dimension matrix M, then we have shown that all the e_i's can be written as linear combinations of the S_i's. Since all the rows of M are orthonormal, by inspection, $MM^T = I$ as in Equation 3.36.

$$\begin{bmatrix} a_0 & a_1 & a_2 & \cdots \\ 0 & a_0 & a_1 & \cdots \\ 0 & 0 & a_0 & \cdots \\ \vdots & \vdots & \vdots & \ddots \end{bmatrix} \begin{bmatrix} a_0 & 0 & 0 & \cdots \\ a_1 & a_0 & 0 & \cdots \\ a_2 & a_1 & a_0 & \cdots \\ \vdots & \vdots & \vdots & \ddots \end{bmatrix} = \begin{bmatrix} 1 & 0 & 0 & \cdots \\ 0 & 1 & 0 & \cdots \\ 0 & 0 & \ddots & \cdots \\ \vdots & \vdots & \vdots & 1 \end{bmatrix} \tag{3.36}$$

If $MM^T = I$, then $M^TM = I$ and $M^TS = I$. Thus, any sequence $f \in \ell^2$ can written as a linear combination of S_i by $f = (fM^T)S$. Hence, the S_i's are complete.

Thus, we have shown in the above proof that the only possible solutions of causal impulse functions $y(t)$ convolving with its anticausal function $y(-t)$ are strictly single impulse functions. That is $y(t) = \delta(t - T) \quad \forall T > 0$ as in Figure 3.9.

We have shown so far that $y(t)$ contains exactly one impulse. We now show that the whitening filter must contain exactly one impulse function at the origin and a nonpolynomial function. First, the whitening filter must contain an impulse. This can be seen in the frequency domain. Since all the density functions of the

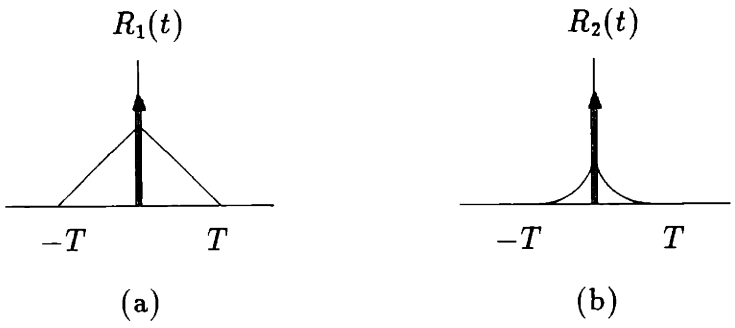

Figure 3.8: Function to Whiten for (a) Synchronous Users, (b) Asynchronous Users.

observation are square-integrable if the the constant (Power Spectral Density of the laser) is subtracted, the spectral factorizations must behave in the same way. They must consist of a constant and a square-integrable function. Its inverse, the whitening filter, must also contain a constant since their product must equal one. Second, due to causality constraints, this impulse must be at the origin. Convolution is a linear operator. Since $w(t)$ also contains an impulse, the only way it can undo a delayed impulse in $y(t)$ is by having a noncausal impulse. But this cannot be since $w(t)$ is causal. Hence, both $y(t)$ and $w(t)$ must contain impulses at the origin. So the form of the whitening filter is known; namely, it consists of an impulse at the origin and a non rational causal function. For the causal wiener filter $h(t)$ in the last section, $C = 1/\sqrt{A}$. The area of the impulse must be $1/\sqrt{A}$, so that $W(f)$ for a large f is $1/\sqrt{A}$, which is necessary to produce a white signal of unit spectral density.

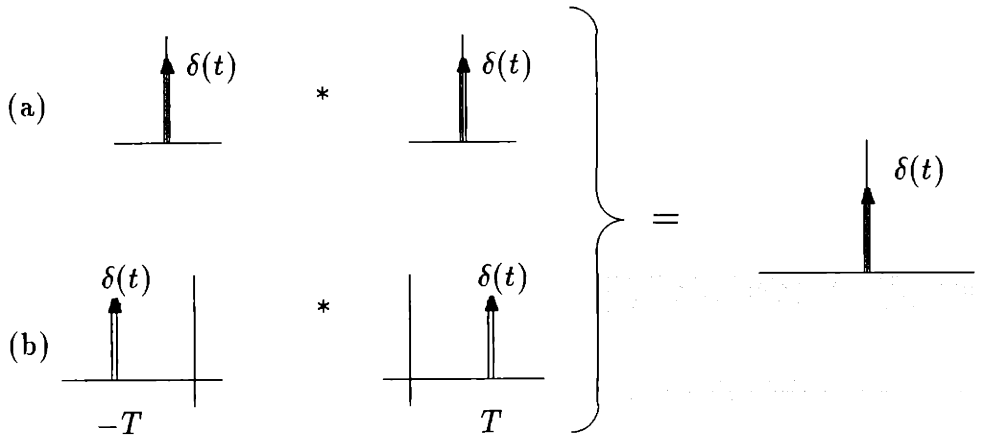

Figure 3.9: Only Possible Causal and Anticausal Impulse Solutions to Impulse Function

3.3 Bounds on Mean Squared Error for Causal Filter

3.3.1 Lower Bounds

The whitening filter is in general difficult to find. From the previous section we found the optimal causal filter $H(f)$ was the filter whose closed loop transfer function was the whitening filter $W(f)$

$$H(f) = \frac{W(f)\sqrt{A}}{1 - W(f)\sqrt{A}} \quad \text{and} \quad W(f) = \frac{H(f)}{1 + H(f)} \cdot \frac{1}{\sqrt{A}} \tag{3.37}$$

where

$$W(f)W(f)^* \left[S_{xx}(f) + S_{nn}(f)\right] = 1 \tag{3.38}$$

Substituting Equation 3.37 into Equation 3.1, the power spectral density of the error can be expressed as a function of the whitening filter.

$$S_{ee}(f) = \left|W(f)\sqrt{A}\right|^2 S_{nn}(f) + \left|1 - W(f)\sqrt{A}\right|^2 S_{xx}(f) \tag{3.39}$$

Given that only $|W(f)|$ is known, but not $W(f)$, $|1 - W(f)|$ can be bounded by

$$|1 - W(f)|^2 = 1 + |W(f)|^2 - 2Re[W(f)] \tag{3.40}$$

$$1 + |W(f)|^2 - 2|W(f)| \leq |1 - W(f)|^2 \leq 1 + |W(f)|^2 + 2|W(f)| \tag{3.41}$$

The MSE can be bounded by substituting the bounds of Equation 3.41 into Equation 3.39 and integrating over all f. The lower bound exists and the the upper bound does not. However, any suboptimal causal filter which gives a finite variance will suffice for an upper bound to the optimal causal filter. The lower bound of the MSE is

$$MSE_{LB} = \int_{-\infty}^{\infty} 2A \left(1 - \sqrt{1 + \frac{1}{A} S_{nn}(f)}\right) df \tag{3.42}$$

Let the integrand be I and by a change of variable, $u_i = i\pi fT \quad i = 1, 2$, and now integrating over u_i,

$$I = 2A \left(1 - \sqrt{1 + \frac{N}{A} S(u_i)}\right) \frac{1}{i\pi T} \tag{3.43}$$

Now we can see the effect of the system parameters on the MSE. Just like the non-causal case, if we increase N, A, V (imbedded in A if we choose to include it, since it is part of the observation and must be whitened along with A), then MSE increases. If T is increased, the MSE decreases. The results hold for both synchronous and asynchronous cases.

Again, in the results section, we will numerically integrate Equation 3.42 to obtain curves for the MSE.

3.3.2 Upper Bounds

Finding a causal and causally invertible whitening filter is in general difficult as we have shown. Suppose the function to whiten is $X(s)$, then $|W(s)|^2 X(s) = 1$, $|W(f)|^2 X(f) = 1$, and $w(t) * w(t) * x(t) = \delta(t)$, where $W(f)$ is the Fourier Transform of $w(t)$ and $W(s)$ is the BLT of $w(t)$. If $X(s)$ were rational, the difficulty lies in factorization. All Power Spectral Densities(BLT) have quadruple symmetry in the

complex plane, so there always exist a spectral factorization (whether it is rational or not). Since the Power Spectral Density must be stable, the region of convergence (ROC) in the complex plane is right of the left most pole and left of the right most pole of the Power Spectral Density. The $j\omega$-axis must be included in the ROC, so the time function can be evaluated along it. Substituting $s = j2\pi f$ into $X(s)$ will give us $X(f)$. However, we transfer to the Bilateral Laplace Transform domain because causality cannot be determined readily from the Fourier Transform.

The BLT for the synchronous and asynchronous noise Power Spectral Density are not rational. Attempts to find a whitening filter by spectral factorization of $S_{nn}(s) + A$ or time domain methods of convolution have been unsuccessful. We can obtain a causal whitening filter for both the noises, but they consist of delays, which does not make it causally invertible (the inverse will consist of an advancement in time to undo the delay).

Hence, we resort to a rational approximation of the Power Spectral Density which will allow us to find the whitening filter of the approximation. The criteria for approximation is to approximate the magnitude of the whitening filter well in the MS sense. Since we are only concerned with $|W(f)|$ and $|1 - W(f)|$, because the MSE needs these functions.

There are no rational functions that can approximate $S_{nn}(s)$ since the the exponential increases faster than any polynomial. The magnitude of the whitening filter is known, so a rational function $|\hat{W}(f)|^2$ can be used to approximate it. Then, substitute $s = j2\pi f$ to obtain $|\hat{W}(s)|^2$ which can be spectrally factored into $\hat{W}(s)\,\hat{W}(-s)$ and the approximate whitening filter $\hat{w}(t)$ can be found (inverse BLT of $|\hat{W}(s)|$). Now, $\hat{w}(t)$ can be nowhere near $w(t)$, and $\hat{W}(s)$ may not even approximate $W(s)$ well in the MS sense, since the complex extension need not be close although the Fourier Transform is close. But it is not so crucial as we are only concerned with the parameter $|W(f)|$ and $|1 - W(f)|$ and $\hat{w}(t)$ will give us good approximate behavior.

3.3.3 Rational Function Approximation

Since the Power Spectral Density of the noise behaves as $\frac{1}{f^2}$, is even and nonnegative for all f, the approximation functions used will be

$$f(x) = \frac{N(x)}{D(x)} \quad \text{with} \quad N(x) = (x^2 - a^2)^2 \quad \text{and} \quad D(x) = [1 + (bx^2)^n]^m \tag{3.44}$$

where n, m are integers and a, b are constants chosen to match first zero in Power Spectral Density. To approximate $S_{n_1 n_1}(f)$ the following function was used

$$\hat{S}_{n_1 n_1}(f) = (N-1)T \frac{[f^2 - (\frac{1}{T})^2]^2}{(\frac{1}{T})^4(1 + (fT)^2)^3} \tag{3.45}$$

and to approximate $S_{n_2 n_2}(f)$

$$\hat{S}_{n_2 n_2}(f) = (N-1)T \frac{[f^2 - (\frac{1}{2T})^2]^2}{(\frac{1}{2T})^4(1 + (f2T)^2)^3} \tag{3.46}$$

Of course there are other better approximations, such as using the same form of rational functions above, but catching more zeros of the power spectral density. But the filter and MSE are harder to find, since the roots must be found in a higher order polynomials.

3.4 Causal Filter for Random Telegraph Wave

Since the power spectral density of the random telegraph wave is a polynomial, the optimal causal filter can be solved for exactly. The lower bound of the causal filter can also be compared to the optimal solution as a measure.

$$W(s)W(-s) = \frac{\frac{2}{T}^2 - s^2}{\frac{4}{T}(N-1) + A(\frac{2}{T}^2 - s^2)} \tag{3.47}$$

$$W(s) = \frac{\frac{2}{T} + s}{\sqrt{A(\frac{2}{T})^2 + \frac{4}{T}(N-1)} + s\sqrt{A}} \tag{3.48}$$

let

$$\alpha = \sqrt{A(\frac{2}{T})^2 + \frac{4}{T}(N-1)} \tag{3.49}$$

$$W(f) = \frac{1}{\sqrt{A}} + \frac{\frac{2}{T} - \frac{\alpha}{\sqrt{A}}}{\frac{\alpha}{\sqrt{A}} + j2\pi f} \tag{3.50}$$

$$w(t) = \frac{1}{\sqrt{A}}\delta(t) + (\frac{2}{T\sqrt{A}} - \frac{\alpha}{A})e^{-\frac{\alpha}{\sqrt{A}}t} \tag{3.51}$$

The whitening filter is an impulse function and exponential as expected. The optimal filter, $h(t)$ is

$$h(t) = \frac{1}{\alpha T - 2}[2\sqrt{A}\delta(t) + T\sqrt{A}\dot{\delta}(t) \tag{3.52}$$

which has an impulse function and differentiator also as expected.

The MSE can be integrated exactly resulting in

$$MSE = \frac{(N-1)}{2T\sqrt{(\frac{1}{T})^2 + (\frac{N-1}{AT})}} + \frac{\sqrt{A}(\alpha - \frac{2}{T}\sqrt{A})^2}{4\alpha} \tag{3.53}$$

3.5 Discussion of Results to RMSE

Results of the numerical integrations for the noncausal, causal lower bound, causal upper bound, optimal filters for synchronous, asynchronous, and random telegraph signal are shown in Figures 3.10, 3.11 and 3.12. The user noise $n(t)$ is dominant over the system noise $v(t)$ so in the integration, we did not include the system noise. Since we have modelled both system noise and laser frequency as white, there is no filter that will give a finite MSE. The white noise model is a mathematical convenience and does not really model reality, since both noises are bandlimited. Hence, the filter will also be bandlimited. Therefore, we could have also included the system noise but bandlimit the integration (the difference in numerical results is negligible).

Looking at the numerical results for the RMSE, we notice that all three user noises have similar results and differ only slightly in MSE. This fact is not surprising since their autocorrelation functions look similar. As the number of users N increases, the MSE degrades approximately with the square root of N. If the spectral height of the laser frequency noise or system noise increases, the MSE also increases as we noticed in the previous sections and which is not surprising.

If the bit time increases, the system performs better, and the MSE decreases. From the system model, this result is expected. Looking at the power spectral densities , we notice that most of the energy of the user noise is located within the main lobe whose bandwidth decreases with increasing T. The laser noise and user noise are independent. Since the laser spectrum is white, the system likes to see all the user noise confined to a small bandwidth. Then anything outside that bandwidth is not corrupted by noise; it comes from the laser and will be guessed perfectly by the system. It is the noise indside that bandwidth that is causing the error. In the limit as $T \rightarrow \infty$, the user noise power spectral density is a delta fuction at the origin, and the system performs great. Physically, when $T \rightarrow \infty$, there is no modulation, so all the noise the other users put on the channel is a DC constant of ± 1, and any random fluctuation belongs to the laser. The system just ignores this constant. Practically, it can also be agreed that the price for better stabilization performance is transmitting at a lower bit rate.

By the same power spectral density argument, it can be concluded that the asynchronous users do more damage to the system that the synchronous users because the bandwidth of asynchronous users is twice that of the synchronous users. Again, from a practical perspective, it can be argued that synchronization is hard to achieve , but the reward is better system performance.

Nevertheless, both these results are counter to our intuition about the stabilization feedback loop. We argued in chapter 2 that modulation was crucial in differentiating our error signal from the other error signals. Hence, quicker bit rate should result in better performance. The same argument holds that asynchronous user noise system works better than synchronous systems because the greater randomness allows better decorrelation with the other bits streams. If, looking at the limit, there were no modulation, then the system would perform bad because there is no way to distinguish each individual error signal.

Finally, the filter itself was interesting. Looking at the power spectral density of

the error signal and knowing that the user noise falls as $1/f^2$, we know that for finite MSE, the filter must increase at least as fast as f. Again, this filter is consistent with the model, since the user noise is located at low frequencies and the laser spectrum is uniform over all frequncies, the system will weight the higher frequencies components much more since they are least corrupted by the user noise. Hence, we expected the high pass filter. However, with our understanding into the circuit, we expected a low pass filter (as mentioned in chapter 2) to filter out all the high frequency user user noise from modulation (sum of all the bit streams).

In conclusion, the results we obtained with the model are consistent with the model, but not with our understanding and intuition of the stabilization circuit itself. Hence, we conclude that Model I does not capture all the characteristics of the physical system. Therefore, a new model is proposed for further analysis.

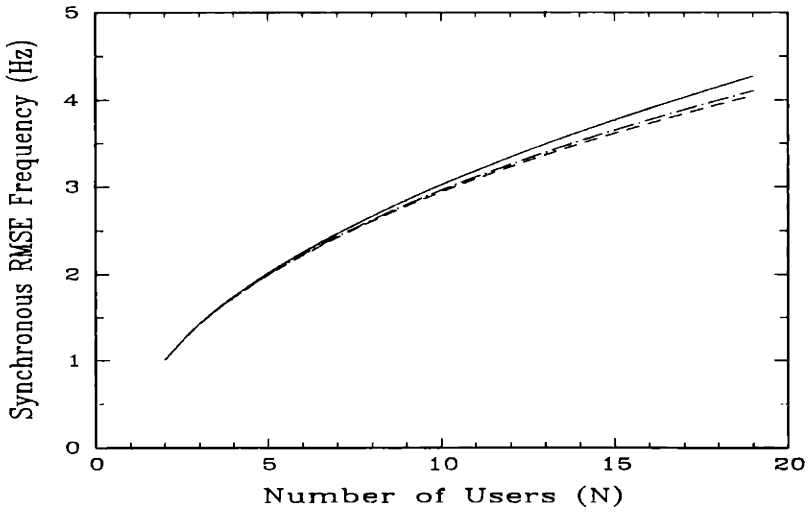

Figure 3.10: MSE for Synchronous users. Solid line is an achievable upper bound to causal optimal filter. Dotted line is a lower bound to causal optimal filter, and the dashed line is the noncausal filter.

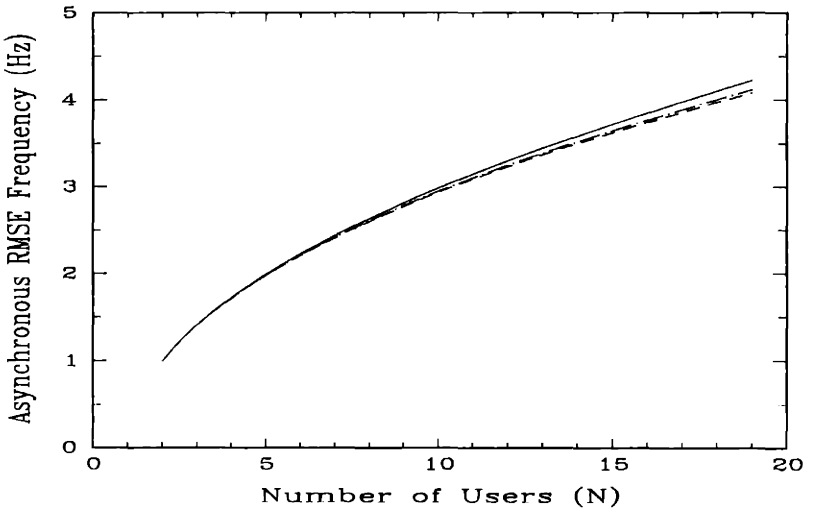

Figure 3.11: MSE for Asynchronous users. Solid line is an achievable upper bound to causal optimal filter. Dotted line is a lower bound to causal optimal filter, and the dashed line is the noncausal filter.

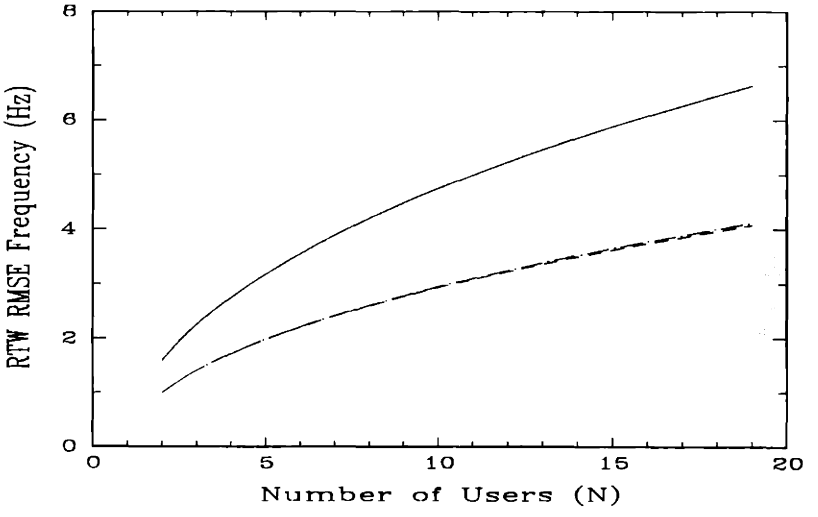

Figure 3.12: MSE for Random Telegraph wave transmission. Solid line is for the causal optimal filter. Dotted line is a lower bound to causal optimal filter, and the dashed line is the noncausal filter.

Chapter 4

System Model II

In Model I, we made two major assumptions. The first assumption is that the error signals are constant. If the offset is removed, the noise in Model I will become will no longer be just a bit stream with constant amplitude, but a bit stream multiplied by a random amplitude. This amplitude is not independent of the data streams and the noise $n(t)$ is not independent of $x(t)$, and Equation 3.1 no longer holds for system model I. From Figure2.5, a new model is proposed to capture the effect of the dependency of the error signals. This model for $N = 2$ users is shown in Figure (4.1). This model describes the experiment more clearly and carefully. When more users are added, they are just connected at the center adder where $v(t)$ is added. This is the point through the photodiode where all the users see the same system and photodiode noise.

For the case $N = 2$, the system model in figure(4.1) can be simplified to the following system in figure(4.2). The simplification was done by looking at all the independent inputs to the system separately. Let

$$F_i(t) = \mathcal{F}^{-1}\left(\frac{1}{1+H(f)}\right) * x_i(t) + \mathcal{F}^{-1}\left(\frac{H(f)}{1+H(f)}\right) * v(t)d_i(t) \qquad (4.1)$$

The system is not linear if there is modulation, but insight can be gained and analysis done. In this reduced model, the effects of the error signals on the other user's error signal can be seen.

For $N = 3$, the system model can be reduced to the following Figure 4.3. Notice

that complexity rapidly increases as N increases, but there is a pattern. For a system with N-users, the following relation is an expression for the error signal of the i-th user. Denote $\mathcal{F}^{-1}$ as the inverse Fourier Transform.

$$e_i d_i = \mathcal{F}^{-1}\left[\frac{1}{1+H(f)}\right] * x_i + \mathcal{F}^{-1}\left[\frac{H(f)}{1+H(f)}\right] * v d_i + \sum_{j\neq i}^{N} \mathcal{F}^{-1}\left[\frac{H(f)}{1+H(f)}\right] * (e_j d_j d_i) \tag{4.2}$$

The error signals of all the users can also be written in matrix notation (letting $K = \mathcal{F}^{-1}\left[\frac{1}{1+H(f)}\right]$ and $L = \mathcal{F}^{-1}\left[\frac{H(f)}{1+H(f)}\right]$, and for notational convenience, we have left out the funtions of time, i.e. $e_i = e_i(t), K = K(t)$, etc.)

$$\begin{bmatrix} e_1 d_1 \\ e_2 d_2 \\ \vdots \\ e_N d_N \end{bmatrix} = \begin{bmatrix} x_1 \\ x_2 \\ \vdots \\ x_N \end{bmatrix} * K + v \begin{bmatrix} d_1 \\ d_2 \\ \vdots \\ d_N \end{bmatrix} * L + \begin{bmatrix} 0 & d_1 & d_1 & \cdots \\ d_2 & 0 & d_2 & \cdots \\ \vdots & & \ddots & \\ d_n & d_n & \cdots & 0 \end{bmatrix} \begin{bmatrix} e_1 d_1 \\ e_2 d_2 \\ \vdots \\ e_N d_N \end{bmatrix} * L \tag{4.3}$$

The error signal must be represented in terms of the data streams $d_i(t)$, the laser frequency noise $x_i(t)$, and the system noise $v(t)$ which are all independent and zero-mean. Then the attempt to find the optimal filter and calculation of the MSE can proceed.

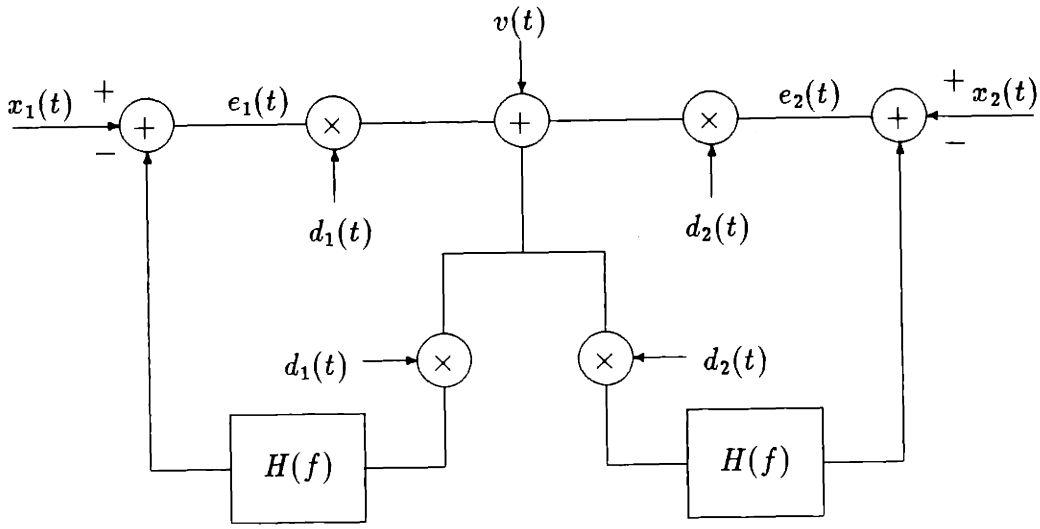

Figure 4.1: Model II of Stabilization System for N=2 Users.

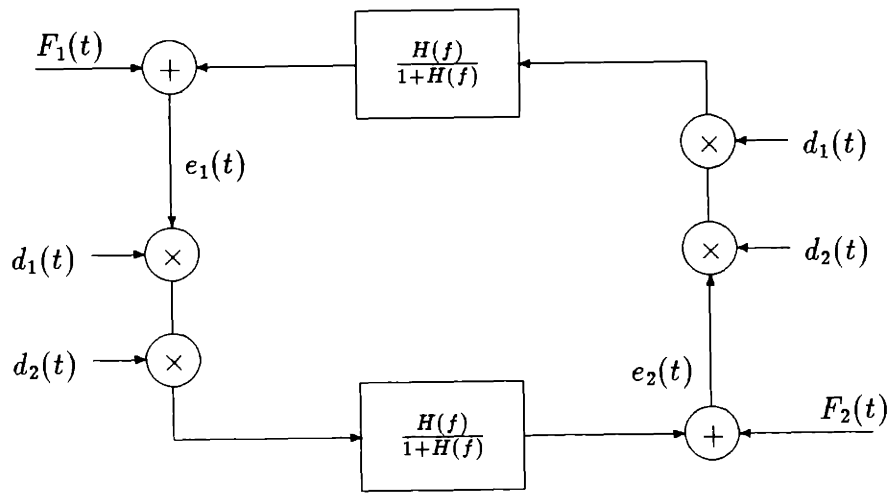

Figure 4.2: Reduction of Model II for N=2 Users

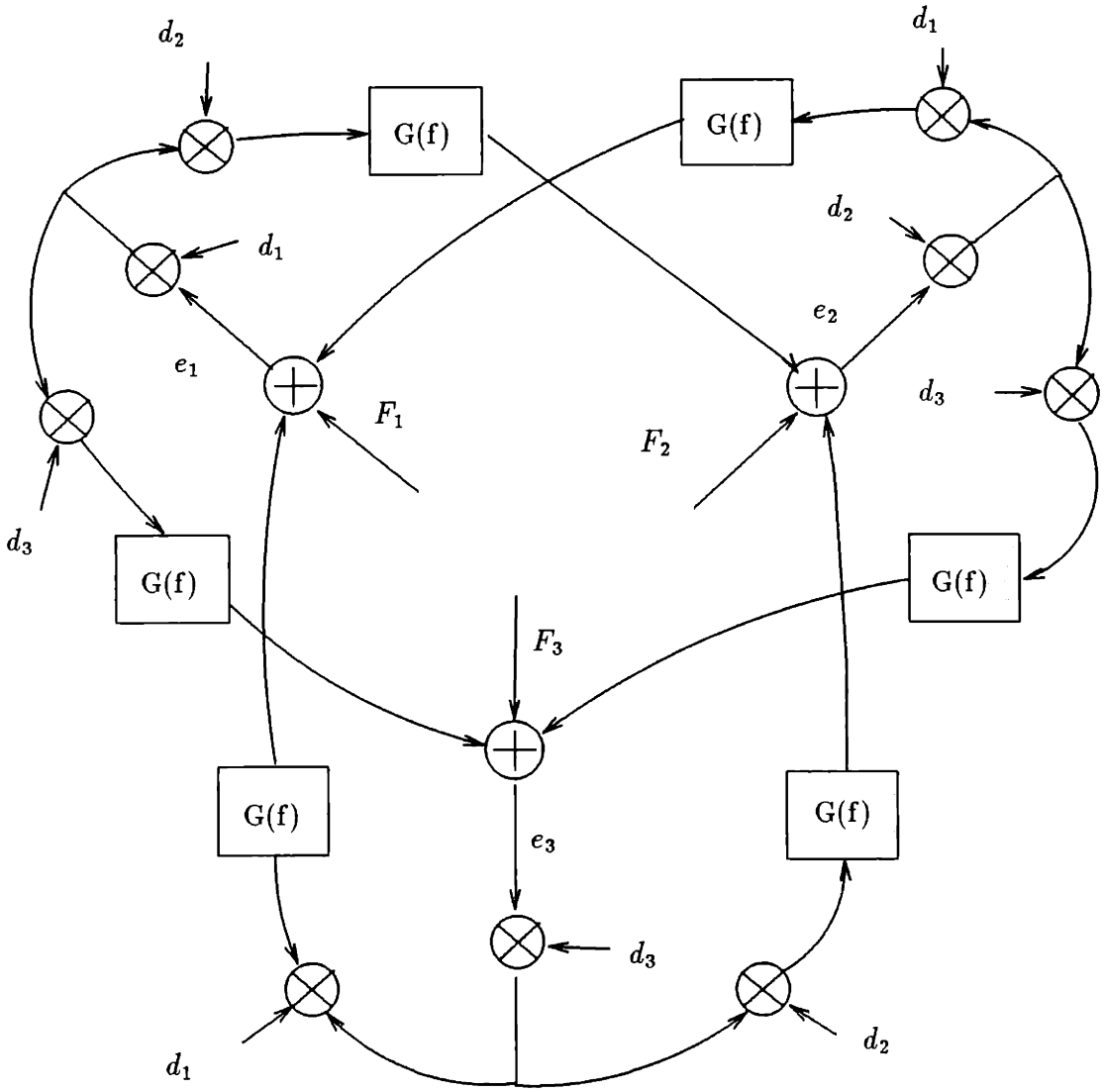

Figure 4.3: Model II Reduction for N=3 Lasers

Chapter 5

Conclusion

5.1 Summary

Optical FDM has the potential to make use of the large available bandwidth in the optical frequencies, but channel frequency monitoring and stabilization is critical to prevent channel interference. Coherent detection offers a number of advantages over Direct Detection, but has stringent linewidth requirements. Thus, frequency stabilization of sources is crucial in optical communication systems.

A frequency stabilization scheme was developed by Glance and built to lock a few optical FDM sources using FSK modulation onto the resonances of a Fabry-Perot robustly. It certainly has the capability to support many more users since there are several resonances of the Fabry-Perot. The system seems like a good candidate for a coherent optical FDM system, and so it is of interest to evaluate the system and its performance.

A reasonable model was developed to study the experimental circuit. From the model and using the MSE of the frequency as the criterion for performance, the optimal filters and bounds to the optimal filters were found. The performance of the stabilization scheme was analyzed in terms of the system parameters. Performance degraded when number of users increased, laser linewidth increased, system noise increased, bit rate increased, and when the users were asynchronous (as opposed to synchronous).

All these results were consistent with the model and our intuition of the model. But the results that the bit rate increase and asynchronous users deteriorate performance did not agree with our intuition and understanding of the stabilization system. Because of the discrepancy, we gained insight into the feedback loop and realized there are limitations to the model.

We realized that the error signals of all the lasers were correlated and our model did not capture the dependency of the error signals. Therefore, we proposed a new model that does capture this dependency for further research. Preliminary work has shown that the behavior of this new model in terms of the system parameters agrees well with our intuition.

5.2 Further Research

There is quite much work to be done on Model II. First, finding the optimal filter is difficult. Second, determining how the system degrades in performance with respect to the number of users is also a challenge.

We used the MSE as the performance criterion. Perhaps there is another measure of system performance that would be more suitable. We assumed that the users were able to initialize onto the correct resonant frequency peaks. In reality, this is very difficult to do. The problem of frequency monitoring the signals is an important problem. Lasers may loose lock and need to be reinitialized onto their resonant peaks. Lastly, the research into the optimal receiver design is important.

References

[1] C. Henry "Theory of the Linewidth of Semiconductor Lasers," *IEEE Journal of Quantum Electronics,* Vol.QE-18, No.11, pp.259-264, February 1982.

[2] B. Daino, et al. "Phase Noise and Spectral Line Shape in Semiconductor Lasers," *IEEE Journal of Quantum Electronics,* Vol.QE-18, No.2, pp.266-270, March 1983.

[3] S.-T. Ho. et al. "Optical Feedback Phase Stabilization of a Semiconductor Laser," *IEEE Journal of Lightwave Technology,* Vol.LT-4, No.3, pp.312-315, March 1986.

[4] G. Glance, et al. "Frequency Stabilization of FDM Signals," *Electronic Letters,* Vol.23, No.23, pp.750-752, 1987.

[5] G. Glance, et al. "Densely Spaced FDM Coherent Star Network With Optical Signals Confined to Equally Spaced Frequencies," *IEEE Journal of Lightwave Technology,* Vol.6, No.11, pp.1770-1781, November 1988.

[6] K. Kikuchi, C.-E. Zah,T.-P. Lee "Amplitude Modulation Sideband Injection Locking Characteristics of Semiconductor Lasers and Their Application," *IEEE Journal of Lightwave Technology,* Vol.6, No.12, pp.1821-1830, December 1988.

[7] H. Cramer and M.R. Leadbetter *Stationary and Related Stochastic Processes,* John Wiley & Sons, Inc., 1955.

[8] A. Papoulis, *Probability, Random Variables, and Stochastic Processes,* McGraw-Hill Book Co., 1984.

[9] H.L. Van Trees, *Detection, Estimation, and Modulation Theory, Part I,* John Wiley and Sons, 1968.